Live imaging of heart tube development in mouse reveals alternating phases of cardiac differentiation and morphogenesis

Kenzo Ivanovitch[1,2], Susana Temiño[1] and Miguel Torres[1,*]

[1]Developmental Biology Program, Centro Nacional de Investigaciones Cardiovasculares (CNIC), Madrid, Spain

[2]Current Address, The Francis Crick Institute, London, UK

Authors ORCID

Miguel Torres: orcid.org/0000-0003-0906-4767

Kenzo Ivanovitch: orcid.org/0000-0003-4706-7686

*Corresponding author: mtorres@cnic.es

ABSTRACT

During vertebrate heart development two progenitor populations, first and second heart fields (FHF, SHF), sequentially contribute to longitudinal subdivisions of the heart tube (HT), with the FHF contributing the left ventricle and part of the atria, and the SHF the rest of the heart. Here we study the dynamics of cardiac differentiation and morphogenesis by tracking individual cells in live analysis of mouse embryos. We report that during an initial phase, FHF precursors differentiate rapidly to form a cardiac crescent, while limited morphogenesis takes place. In a second phase, no differentiation occurs while extensive morphogenesis, including splanchnic mesoderm sliding over the endoderm, results in HT formation. In a third phase, cardiac precursor differentiation resumes and contributes to SHF-derived regions and the dorsal closure of the HT. These results reveal tissue-level coordination between morphogenesis and differentiation during HT formation and provide a new framework to understand heart development.

INTRODUCTION

The heart is the first organ to form and function during embryonic development. At embryonic day (E) 7.5, cardiac precursors in the splanchnic mesoderm (mesoderm apposed to the endoderm) differentiate into cardiomyocytes by assembling the contractile sarcomere machinery (Tyser et al., 2016) and form a bilateral structure known as the cardiac crescent (cc) in the mouse. Concomitant with foregut invagination, the cc swings inwards to become placed underneath the developing head folds. By a complex morphogenetic process, the cc subsequently transforms into an early heart tube (HT) initially opened dorsally, which by E8.25 has transformed into a closed and beating linear HT, also known as the primitive HT (Evans et al., 2010; Kelly et al., 2014).

The cc and early HT mainly give rise to the left ventricle (Zaffran et al., 2004). The right ventricle (RV), the outflow tract and most of the atria derive instead from cardiac progenitors located dorso-medially to the cc in the splanchnic mesoderm, that are progressively recruited at the poles of the HT at subsequent developmental stages (Cai et al., 2003; Kelly et al., 2001; Mjaatvedt et al., 2001; Waldo et al., 2001; Galli et al., 2008 135:1157-67). These findings led to the concept that cardiac mesodermal

progenitors contain two populations of cells: the first heart field (FHF) precursors, recruited early in development to form the initial HT and mostly containing the LV primordium, and the second heart field (SHF), recruited later and elongating the HT (Buckingham et al., 2005).

Clonal analysis (Devine et al., 2014; Lescroart et al., 2014; Meilhac et al., 2004a) supports the idea that FHF and SHF precursors are two independent developmental fields with dedicated molecular pathways. Clonal analysis also showed that the SHF shares a common origin with the skeletal muscles of the head and neck within the pharyngeal mesoderm (Lescroart et al. 2010, Lescroart et al. 2015), further supporting differences between FHF and SHF populations. However, the existence of a common precursor between FHF and SHF was also reported in the early mouse embryo (Meilhac et al., 2004a) and other views suggest that the heart would form by a continuous differentiation process from a single population of cardiac precursors and only timing of recruitment would distinguish cells of the FHF and SHF (Abu-Issa et al., 2004; Moorman et al., 2007). In support of the latter, the typical marker of the SHF, Islet1 (Cai et al., 2003), is also transiently expressed in FHF precursors and must therefore be considered as widespread cardiac progenitor marker instead (Cai et al., 2003; Prall et al., 2007; Yuan and Schoenwolf, 2000). Whether the recruitment of cardiomyocytes from progenitors is a continuous process and how this coordinates with morphogenesis, however, has not been directly studied. This is partly because the spatial arrangement of progenitors and differentiated cardiomyocytes has so far been analyzed on fixed embryos (Cai et al., 2003; Spater et al., 2013) and the expression dynamics of genes reporting differentiation together with cell movements during HT morphogenesis have not been captured so far (Abu-Issa, 2014).

Here, we report the live-imaging and 3D+t cell tracking of HT formation in whole mouse embryos. Using this method, in conjunction with an Nkx2.5eGFP reporter line, which provides high level of GFP in differentiated cardiomyocytes, we studied the dynamics of cardiac field differentiation. During an initial phase, FHF cardiac precursors differentiate rapidly to form a cardiac crescent, while limited morphogenesis takes place. During a second phase, no differentiation events are detected and extensive morphogenesis, including splanchnic mesoderm sliding over the endoderm, results in HT formation. Finally, using an Isl1-Cre lineage tracing assay combined with live-imaging, we show that during a third phase, cardiac

84 precursor differentiation resumes and contributes not only to the known SHF-derived
85 regions but also to the dorsal aspect of the HT. These results show essential properties
86 of FHF and SHF contribution to heart development and reveal tissue-level
87 coordination between alternating phases of differentiation and morphogenesis during
88 HT formation.

89

90 **RESULTS**

91

92 **3D static analysis of mouse HT formation**

93 To assess how the initial cardiogenic region transforms into a HT and differentiates,
94 we first analyzed *Nkx2.5*$^{cre/+}$; *Rosa26Rtdtomato*$^{+/-}$ embryos, in which both cardiac
95 precursors and cardiomyocytes are labeled (Stanley et al., 2002). Before cc
96 differentiation, at early head fold stage (EHF, ~E7.5), the cardiogenic region is
97 visualized as a flat horse shoe-shaped tdtomato+ mesodermal layer at the rostral
98 border of the embryo (Figure 1A, A', and Video 1). Figure 1-figure supplement-1
99 shows the criteria for embryo staging (Downs and Davies, 1993; Lawson, 2016). In
100 the *Nkx2.5*$^{cre/+}$*; Rosa26Rtdtomato*$^{+/-}$ embryos, tdtomato labeling is also observed in the
101 endocardium and endothelial cells (Stanley et al., 2002) but not in the endoderm
102 (Figure 1-figure supplement 2A, A'). We next studied the distribution of Cardiac
103 troponin T (cTnnT), one of the first evident sarcomeric proteins to appear in the
104 cardiac crescent (Tyser et al., 2016). At EHF stage (Figure 1B), while most embryos
105 are negative for cTnnT expression, some embryos show weak cTnnT localization in
106 subsets of cells (Figure 1-figure supplement 3A, A'). At a subsequent embryonic
107 stage (~E7.7), cTnnT signal reveals the cc, which is folding inwards. During folding,
108 the cTnnT signal increases. cTnnT+ cells are initially columnar epithelial cells and
109 show apical localization of the tight junction component zona-occluden-1 (ZO-1)
110 (Figure 1-figure supplement 3B, B'). During differentiation, cardiac precursors switch
111 to a rounded shape (Linask et al., 1997) (Figure 1C, D) and separate from the
112 endoderm, while maintaining a basal lamina at the endocardial side (inset in Figure
113 1D and Figure 2D). Morphogenetic changes starting at ~E8 subsequently lead to the
114 formation of a hemi-tube whose major axis is transversal to the embryo A-P axis. We
115 will refer to this stage as transversal HT (Figure 1E). Later, the tube adopts a more

116 spherical shape, very similar to the linear HT but still open dorsally. We will refer to
117 this stage as open HT (Figure 1F). The HT eventually closes dorsally (Figure 1G, red
118 arrows in Figure 1G'') and a prominent arterial pole (prospective RV) (Zaffran et al.,
119 2004) becomes visible, completing linear HT formation by ~E8.25 (yellow arrows in
120 Figure 1G'', Figure 1H, see also Video 2).

121 To assess the overall growth of the forming HT, we measured cTnnT+ tissue volume
122 in segmented z-stacks, at the stages described above (Figure 1I and Supplementary
123 file 1). During the first phase of cardiomyocyte differentiation, the cTnnT signal
124 expands resulting in a cardiac crescent rapidly doubling in volume (Figure 1C', D', I).
125 During the subsequent phase of morphogenesis, from cc to open HT stage, growth is
126 less pronounced despite extensive morphological changes (Figure 1E', F', I). The
127 Volume of the HT appears to increase again upon addition of the RV primordium to
128 the arterial pole and dorsal HT closure (Figure 1G', I). HT growth likely reflects an
129 increase in cell number occurring during the formation of the heart tube.
130 Cardiomyocytes are proliferative at this stage (de Boer et al., 2012), and we can
131 indeed observe mitotic figures in the HT (Figure 1J). From this analysis, however, it
132 is unclear how much of the growth observed is due to cardiomyocyte proliferation
133 versus addition of new cardiomyocytes from cardiac progenitor cells located in the
134 splanchnic mesoderm.

135

136 **3D analysis of cardiac progenitor differentiation**

137 To visualize the boundary where cardiac progenitors abut differentiating
138 cardiomyocytes during HT morphogenesis, we immunostained *Nkx2.5*$^{cre/+}$
139 *Rosa26Rtdtomato*$^{+/-}$ embryos at the transversal-HT stage with the differentiation
140 marker cTnnT and acquired whole-mount images (Figure 2A). Cre activation of
141 tdtomato was detected in both the FHF and SHF, as well as in the endoderm and
142 endocardium (see optical sections in Figure 2A', A'', F, F' and Figure 2-figure
143 supplement 1A) (Stanley et al. 2002). Cardiomyocytes are separated from the
144 endoderm by the endocardium. In contrast, undifferentiated cardiac precursors lie
145 medio-dorsally in direct contact with the endoderm in areas where endocardial cells
146 are not detected (Figure 2A', A''). This is confirmed by the absence of the endothelial
147 marker CD31 (Figure 2-figure supplement 1A, B, B'). We then rendered in 3D the

148 *Nkx2.5*^{cre}-labeled lineages, including both FHF and SHF, and the cTnnT+ tissues,
149 including only the FHF/cc, which allowed visualizing the boundary between SHF and
150 cc at the tissue level (Figure 2A, B, B', Figure 2-figure supplement 2A', Video 3 and
151 see material and methods –non-cardiac tdtomato signal was removed manually–).

152 To identify the changes associated to cardiomyocyte differentiation at the cellular
153 level, we labeled single cells with membrane-GFP (see Material and Methods).
154 cTnnT- progenitors have an epithelial-like columnar cell shape, while the
155 differentiated cTnnT+ cardiomyocytes are rounder and have lost the columnar
156 epithelial organization (Figure 2C-E and Figure 2-source data 1). This is reminiscent
157 of the cell shape transition observed in the distal outflow tract (OFT) at later stages of
158 heart development, when SHF progenitor-to-cardiomyocyte differentiation takes
159 place (Francou et al., 2014; Ramsbottom et al., 2014; Sinha et al., 2012). Interestingly,
160 some cells at the boundary zone exhibit weak cTnnT localization and yet show
161 columnar shapes typical of mesodermal cardiac precursors (Figure 2F-F'''' and red
162 arrows in Figure 2F''', F''''). Unlike differentiated cardiomyocytes, these cells do not
163 show rounded shapes, and therefore they may represent a transient state between
164 progenitors and differentiated cardiomyocytes; however, the nature of such state
165 cannot be addressed by static analysis. Differentiation of cardiac progenitors is thus
166 accompanied by changes in cell shape and detachment from the endoderm.

167 We next assessed the expression pattern of the *Nkx2.5eGFP* enhancer reporter line, in
168 which GFP expression is restricted to cardiomyocytes (Lien et al., 1999; Prall et al.,
169 2007; Wu et al., 2006). To characterize this reporter line in detail, we immunostained
170 *Nkx2.5eGFP* embryos against cTnnT, (Figure 3A, B and Figure 3- figure supplement
171 1A, B) and compared the relative intensities of cTnnT and GFP in manually-
172 segmented single cells (Figure 3C, D Figure 3-figure supplement 2A and Figure 3-
173 source data 1). We found that the GFP level varied linearly with cTnnT level (Figure
174 3D), although considerable variability of GPF levels was observed within each
175 cTnnT+ and cTnnT- cell population. Scoring of a large number of cells allowed to
176 reproducibly identify the top 50% GFP-expressing cells as positive for cTnnT+
177 (Figure 3-source data 1). Genetic tracing experiments using the *Nkx2.5*$^{cre/+}$
178 *Rosa26Rtdtomato*$^{+/-}$ line instead show strong tdtomato level in both the FHF and SHF
179 (Figure 3- figure supplement 3A).

180 We next characterized the boundary between cardiomyocytes and cardiac precursors

181 in transversal HT stage embryos of the *Nkx2.5eGFP* reporter line. We measured mean
182 fluorescent intensity in manually segmented cells at the boundary zone and found that
183 GFP level and cTnnT signals correlate at the individual-cell level (Figure 3B', E,
184 Figure 3-figure supplement 2B, C and Figure 3-source data 1). Altogether, these
185 results indicate that the *Nkx2.5-eGFP* reporter is suitable for tracking cardiomyocytes
186 in live-imaging and reliably identifies the top 50% GFP-expressing cells as cTnnT-
187 positive.

188

189 **2-photon live-imaging of early cardiac development in the mouse embryo reveals**
190 **morphogenetic events leading to HT formation**

191 We next established a live-imaging method to dynamically characterize the formation
192 of the HT in the mouse embryo (Figure 4A) (Chen et al., 2014). We adapted a
193 previously reported culture system (Nonaka, 2009; Nonaka et al., 2002) in which the
194 whole mouse embryo is immobilized by inserting the extraembryonic region in a
195 holder (Figure 4C). After culture, embryos showed normal morphology, their hearts
196 were beating and circulation was initiated (Figure 4D, E and Video 4). This culture
197 system in combination with two-photon microscopy enabled the generation of high-
198 resolution 3D+t videos (Figure 3B and see Methods and Materials). Maximum culture
199 time and imaging achieved was 24 hours (Figure 4-figure supplement 1A, n=3).
200 However, typical acquisition times varied in most cases between 3 and 13 hours. The
201 rate of acquisition varied in most cases between 4 and 9 minutes, with some
202 exceptions depending on the specific aim of the recording (see video legends).

203 Imaging *Mesp1*$^{cre/+}$*; Rosa26Rtdtomato*$^{+/-}$ embryos allowed tracking the anterior
204 mesoderm (Saga et al., 1996; Saga et al., 1999), including cardiac lineages, from cc
205 stage up to HT stage (Figure 4F, F' and Videos 5-6). The time-lapse analysis provided
206 insight on the formation of the endocardial lumen (Figure 4F', F''). The endocardium
207 is initially observed as a bilayer of cells and eventually splits into dorsal and ventral
208 layers, which move apart from each other allowing the lumen to become visible
209 between the layers (see Videos 6 and 7 for confocal views and video 8 for a bright
210 field view). Thin cytoplasmic bridges between the endocardial layers persist and
211 extend as the endocardial layers separate from each other (see white arrows in Figure
212 4F' and Video 6). Heartbeat becomes detectable around this stage and circulation in

213 the embryo is then initiated.

214 Imaging *Nkx2.5*$^{cre/+}$*; Rosa26RmT/mG*$^{+/-}$ embryos, in which Cre-recombined cells
215 activate membrane-bound GFP, we could track cells during differentiation, as they
216 transit from a columnar to a round shape and start contracting (Figure 4G-G'', Video
217 7 and bright-field Video 8). We found that the endocardial lumen started to appear
218 while cc cells still remained columnar (compare time points 2h 13m and 3h 48m in
219 Figure 4G'). Cell rounding is therefore unlikely to initiate the formation of the
220 cardiovascular lumen.

221 Interestingly, this analysis also showed that the transformation of the cc into the HT
222 involves the antero-medial displacement of the splanchnic mesoderm (white arrows in
223 Figure 4F, F'). This displacement promotes the folding of the cardiac crescent into a
224 hemi-tube by bringing closer the future borders between the HT and the mesocardium
225 (see yellow lines in Figure 4F' indicating the distance between the borders at different
226 times). These borders coincide with the frontiers between cardiomyocytes and
227 undifferentiated splanchnic mesoderm (see details in Videos 7, 17 and Figure 7A',
228 A''). Interestingly, the movement of the splanchnic mesoderm is not coherent with
229 the endoderm but a relative displacement is detected between the two layers (Video 9).
230 Estimation of splanchnic mesoderm displacement speed towards the midline from
231 time-lapse analyses (Figure 4F', and Video 6) indicates a range of average speeds
232 from 12 to 20 μm/hour (15.8 +/-2.4 μm/hour, mean +/- SD, n=3, Figure 4-figure
233 supplement 2 and Figure 4-source data 1). These measurements estimate that midline
234 convergence of the splanchnic mesoderm takes approximately 5-7 hours from the late
235 cc stage until the open HT stage (Figure 4-figure supplement 2).

236 Our results show the feasibility of live time-lapse analysis of mouse HT formation
237 and reveal that splanchnic mesoderm displacement, at least in part by sliding over the
238 endoderm, is an essential aspect of HT morphogenesis.

239

240 **Live tracking of Cardiomyocyte differentiation in individual cells reveals cardiac**
241 **crescent differentiation dynamics.**

242 Next, to specifically track cardiac differentiation, we used the *Nkx2.5eGFP* live
243 reporter. We first studied the general activation pattern of this reporter in live analysis.
244 At E7/bud stage, a faint and scattered GFP signal is detected in proximity to the yolk

245 sack, at the anterior border of the embryo (Figure 5-figure supplement 1A). At neural
246 plate stage, just prior to the ventral folding of the embryo, the GFP signal remains
247 weak but spreads to delineate a crescent in the anterior region of the embryo (Figure
248 5-figure supplement 1A and Video 10). During about 5-6 hours starting at the EHF
249 stage, the GFP signal increases in intensity, which correlates with the previous
250 observations on cTnnT activation (Figure 4H, Figure 1C and Video 11). From
251 transversal to open HT (5-7 hours) and from the open HT to HT (2-3 hours) the GFP
252 signal remains stable (Figure 5-figure supplement 1B, B', C, C' and Video 12). We
253 conclude that an increase in GFP level in *Nkx2.5eGFP* embryos reports
254 cardiomyocyte differentiation. In addition, these results reveal the timing of the main
255 phases of linear HT development; cc differentiation, formation of the open HT and
256 dorsal closure (Figure 4I).

257 We next sought to track the trajectories and differentiation of individual cardiac
258 precursors within the entire cardiogenic region by 3D+t live imaging. To this end, we
259 used the *Polr2a*^{CreERT2} (*RERT*) allele (Guerra et al., 2003), which provides ubiquitous
260 tamoxifen-inducible Cre activity in combination with a *Rosa26Rtdtomato* reporter.
261 We then titrated the tamoxifen dose for a labeling density that would allow single cell
262 tracking during prolonged time-lapse analysis and combined this with the
263 *Nkx2.5eGFP* reporter (see materials and methods). Typically, for each video, we
264 acquired z-slices every 3-5µm achieving a total z-depth of 200µm – with some
265 variations depending on the stage considered- and manually tracked in 3D+t for
266 several hours an initial population of ~50 to ~100 cells per video, which represents
267 around 5-10% of the total number of cells present in the cc (de Boer et al., 2012).

268 We first tracked cells of the cardiac forming region starting at EHF stage –when
269 cardiac precursors are undifferentiated– up to stages in which cardiomyocytes have
270 differentiated in the cc but the transversal HT stage has not been reached yet (Figure
271 5A and Figure 5-source data 1). At the onset of cardiac differentiation, the cardiac
272 crescent swings ventrally concomitant with foregut pocket formation. During this
273 movement we found that the relative positions of the cardiac progenitors are
274 maintained from the initial stage through the differentiated cc (Video 13). Relative
275 cell positions therefore remain mostly coherent as the embryonic tissues undergo this
276 initial global movement. Differentiation events are detected in some of the tracked
277 cells by cell shape change from columnar to rounded and by the increase in GFP

278 signal (see example in Figure 5B, D and Figure 5-source data 1). In contrast, other
279 tracked cells located in the splanchnic mesoderm remain in contact with the endoderm,
280 retain a columnar shape and show low GFP level throughout the videos (Figure 5C).
281 These cells are likely to be SHF cardiac progenitors and not endocardial cells, which
282 are not present in this area (Figure 2-figure supplement 2A, B, B'). Endocardial cells
283 are instead present in the cardiac crescent and have typical elongated spindle-like
284 shapes (Figure 4F and Figure 5-figure supplement 3A).

285 Next, in order to establish a fate map of the cardiac forming region at the EHF stage,
286 we tracked back in time the population of cells that showed high GFP intensity (top
287 50%) at the end of the video (Figure 5F, H and Figure 5-source data 1). According to
288 our previous analysis (Figure 3D), these cells can reliably be assigned to
289 cardiomyocytes. The initial location of this cell population fated to become cc
290 cardiomyocytes delineates a crescent-shaped domain at EHF stage (Figure 5H). Cells
291 retaining lower GFP intensity level throughout the video initially localize posteriorly
292 and medially to this crescent. Most of the cells that have high GFP levels at the final
293 time point show low GFP levels at the initial time point and increase their GFP level
294 over time (Figure 5E-G and Figure 5-source data 1). These results suggest that
295 cardiomyocytes of the cc differentiate during 5-6 hours starting at the EHF stage,
296 which is consistent with the onset of detectable cTnnT at that stage (Figure 1B and
297 Figure 1-figure supplement 2A, A').

298 Cells in the cardiac mesoderm do divide during the observation time, so we identified
299 cell division events and tracked the descendant cells. 43% of the tracked cells
300 underwent one division during the 4-5 hour videos. To determine whether cell fate
301 (differentiation versus progenitor) is allocated in the cardiogenic mesoderm at the
302 EHF stage, we tracked GFP levels in dividing cells and their descendants. We found
303 that most sister cell pairs show matched high or low GFP intensity levels at the end of
304 the observation period (38 out of 39, Figure 5I, Figure 5-figure supplement 2A-D and
305 Figure 5-source data 1). This observation suggests that commitment of cardiac
306 precursors to differentiation is already established by the EHF stage and largely
307 transmitted by lineage.

308

309 **Cardiomyocyte differentiation is not detected during heart tube morphogenesis.**

310 We next studied cardiac differentiation dynamics during subsequent stages when the
311 cc transforms into the HT by extensive morphogenesis. To do so, we tracked cells
312 located in the splanchnic mesoderm and cc in *Nkx2.5-eGFP* embryos at successive
313 periods of around 3 hours covering the 5-7 hours during which the transversal HT
314 transforms into the open HT (Figure 6A, B, E, Video 14 and Figure 4-source data 1).
315 This analysis revealed that the trajectories of cc cells move apart from each other over
316 time as the tissue expands during the transition from the transverse HT to the more
317 spherical open HT. The HT starts to beat during the observation period, especially at
318 the later stages, and therefore, in some cases, cardiomyocyte cell shape appears
319 distorted in single optical sections (Figure 6F), however the GFP level could be
320 determined. As mentioned above, antero-medial movement of the splanchnic
321 mesoderm can be observed concomitant with the transformation of the transversal HT
322 into the open HT (visible also in Video 5 and 12). We found that cells with high GFP
323 level at the initial time points –differentiated cardiomyocytes– retain rather stable
324 GFP levels (green tracks in Figure 6C, D, G and Figure 6-source data 1). In addition,
325 all cells that initially showed low GFP levels did not increase GFP intensity during
326 time-lapse; thus new events of cardiac differentiation were not detectable by this
327 approach (red tracks in Figure 6C, D). Tracking cells for longer periods of time,
328 covering from cc differentiation continuously up to the open HT stage, confirmed that
329 cc differentiation is followed by a period of time in which no differentiation events
330 occur (Figure 6- figure supplement1, n=19 cells tracked in one embryo).

331 To confirm the absence of detectable cardiac differentiation events during this period,
332 we next focused on the live analysis of cells located at the boundary between
333 cardiomyocytes and undifferentiated splanchnic mesoderm. As expected, we observed
334 GFP-low cells located adjacent to GFP-high cells in the boundary zone (Figure 6H
335 and Video 14). Those cells retain stable GFP levels throughout the tracking time and
336 did not increase their GFP level (Figure 6I, boundary imaged 20 times in different
337 locations and in 6 independent embryos). Importantly, they retain a columnar shape
338 typical of weak cTnnT+ and cTnnT- cells located at the boundary zone (see Figure
339 2F'' and Figure 3B'). Although these cells migrate antero-medially relative to the
340 underlying more static endodermal cells (see endodermal cell highlighted by the red
341 arrow from t=69m in video 9), they do not contribute to the HT during the
342 observation period. We confirmed this observation in longer time-lapse videos

343 spanning 7 hours that covered the whole transition from transversal to open HT stage.
344 Again, progenitors strictly respected the boundary with the HT throughout the entire
345 time-lapse video (Figure 7A-A''' and Video 15, boundary imaged 5 times in distinct
346 locations and in 2 independent embryos). All together, these data suggest that during
347 the transformation of the cc into the dorsally open HT no cardiomyocytes are added to
348 the HT from the SHF. These observations suggest two distinct phases of early HT
349 formation: a first phase of differentiation of the FHF into the cc, lasting around 5
350 hours, and a second phase of HT morphogenesis in which the SHF progenitors remain
351 undifferentiated, lasting around 5-7 hours. During this second phase, extensive
352 remodeling of the cardiac crescent is concomitant with the antero-medial splanchnic
353 mesoderm displacement.

354

355 **Imaging the Isl1-expressing cell lineage confirms absence of cardiac progenitor**
356 **differentiation during early heart tube morphogenesis.**

357 The LIM domain transcription factor Islet1 (Isl1) is a cardiac progenitor marker. Its
358 expression is transient in the precursors of the cc, while it remains expressed in SHF
359 progenitors for an extended period (Brade et al., 2007; Prall et al., 2007, Yuan and
360 Schoenwolf, 2000). Cells of the *Isl1*-expressing lineage detected with Cre reporters
361 therefore contribute only scarcely to the cc, while extensively to the SHF and its
362 derivatives (Cai et al., 2003; Ma et al., 2008). To test these observations in live
363 imaging, we combined *Nkx2.5eGFP* with tracing of the *Isl1* cell lineage using the
364 *Isl1*^{cre} driver and the *Rosa26Rtdtomato* reporter. We found that tdtomato labeling is
365 first detectable in scarce isolated cells of the GFP+ cc during the period when the cc
366 swings ventrally and differentiates (from t=2h 36m to t=4h in Figure 8A, B). In
367 contrast, a dense tdtomato labeling appears in the GFP-low cells of the splanchnic
368 mesoderm as the cardiac crescent fully differentiates (from t=2h24m to t=4h in Figure
369 8A and C and Video 16). tdtomato is as well detected in the endoderm and
370 endocardium (not shown). Consistently with previous reports (Cai et al., 2003),
371 *Isl1*^{cre}-induced recombination detected in live analysis is thus low in the cc and
372 complete in the SHF.

373 Once the cc is formed, if cells of the SHF would continuously differentiate, then
374 regions of the forming heart tube contributed by the SHF precursors should appear

375 densely co-labeled with both GFP and tdtomato. Live imaging shows instead that
376 tdtomato+ cells establish a boundary with GFP+ cells, confirming no signs of
377 differentiation of SHF precursors during the observation period (Figure 8A, C and
378 Videos 17). The live imaging, however, did not allow to unambiguously identify all
379 cells located deep inside the live tissue at the final stages recorded. The arterial pole
380 in particular is located deep in the embryo. It is therefore challenging to accurately
381 track cardiac differentiation by the increase of GFP levels there (Figure 8-figure
382 supplement 1A-A'', from around 200µm depth, see next section). To overcome these
383 limitations, we fixed and immunostained embryos against cTnnT after completion of
384 the live-imaging experiments, and imaged them by 3D confocal microscopy. No solid
385 domains containing double-labeled cells were detected, indicating that progenitors
386 located in the SHF did not undergo differentiation in the boundary zone from cc to
387 open HT stage (Figure 8D). These results are consistent with the single-cell tracking
388 analysis and confirm that the SHF does not differentiate during linear HT
389 morphogenesis.

390

391 **Cardiac differentiation is detected during the late stages of HT development.**

392 We next wanted to determine when cardiac progenitors located in the SHF start to
393 differentiate. In order to address the timing of SHF contribution to the arterial pole,
394 we next fixed and optically cleared *Nkx2.5eGFP*; *Ils1*$^{cre/+}$; *Rosa26Rtdtomato*$^{+/-}$
395 embryos at different stages from cc up to heart looping (n=10) and assessed the
396 appearance of GFP and tdtomato double-positive domains in the HT. In agreement
397 with our previous observations, we found that SHF cells do not differentiate up to the
398 open HT stage, when the dorsal seam of the heart is still open. In contrast, massive
399 appearance of solid domains of double positive cells is observed subsequently in the
400 fully closed HT, reinforcing our previous interpretation (Figure 9A, B and Videos 19-
401 20). At this stage, the primordium of the RV has been added at the arterial pole
402 (Zaffran et al., 2004, Laugwitz et al., 2005, Moretti et al., 2006) and is fully composed
403 of double-positive cells. The dorsal seam of the HT is also densely populated by
404 double-positive cells, indicating a contribution of precursors from the splanchnic
405 mesoderm to the cardiomyocyte population that finalizes the dorsal closure of the
406 linear HT.

407 In order to capture the initiation of SHF contribution to the HT by live imaging, we
408 first focused on the venous pole, as this region is more directly exposed than the rest
409 of the HT and therefore more suitable for live-imaging. In videos that captured the
410 transition from the open HT to the closed linear HT, some cells at the border between
411 the FHF and SHF maintain low GFP levels during the first part of the recording and
412 upregulate GFP to the level of the cardiomyocyte population as the HT forms (Figure
413 8-figure supplement 2). We next aimed to live-track the activation of SHF
414 differentiation at the arterial pole. Because of the imaging limitations in this area,
415 quantitative analysis of the GFP signal was not possible and we instead used the
416 qualitative detection of SHF cells addition to the HT. To achieve this, we imaged an
417 *Nkx2.5eGFP*; *Ils1*$^{cre/+}$; *Rosa26Rtdtomato*$^{+/-}$ embryo at successive time points
418 throughout the transition from open to linear HT and tracked tdtomato+ cells
419 incorporation to the HT at the arterial pole. This study further confirmed that SHF
420 differentiation at the arterial pole is initiated when the HT is about to close dorsally
421 but not before (Figure 9C). Thus, SHF cells do not differentiate during the 5-7 hour
422 period when morphogenesis of the open HT takes place, but coordinately start
423 differentiation at different regions of the HT during dorsal closure. Interestingly, these
424 regions do not only include arterial and venous poles but also the dorsal seam of the
425 HT.

426

427 **DISCUSSION**

428

429 Here we established a whole-embryo live-imaging method based on two-photon
430 microscopy that allows whole-tissue tracking at cellular resolution. By combining
431 various genetic tracing tools, we labeled progenitor and differentiated cardiomyocytes
432 and performed 3D cell tracking over time combined with 3D reconstruction of the HT
433 at multiple stages. We report three distinct temporal phases of HT formation (Figure
434 10). During the first phase, the cc differentiates rapidly and morphogenesis, in terms
435 of changes in the relative position of cells, is minimal. During the second phase,
436 differentiation is not detected and morphogenetic remodeling gives rise to a dorsally
437 open HT. During the third phase, cardiac precursor recruitment and differentiation
438 resumes, contributing to the formation of the RV and the dorsal closure of the HT.
439 Our results support the early establishment of distinct FHF and SHF cell populations

440 and show that the morphogenetic changes that transform the cc into a HT largely take
441 place in the absence of cardiac precursor differentiation. These observations indicate
442 tissue-level coordination of differentiation and morphogenesis during early
443 cardiogenesis in the mouse.

444 The series of 3D reconstructions from fixed embryos was important to establish a
445 reference staging of HT formation. This allowed us to accurately stage embryos in
446 live experiments based on morphology and it will also be useful in the future for gene
447 expression mapping and accurate phenotypic analysis of mutant embryos. The tissue
448 growth pattern observed in static 3D reconstructions was insightful to suggest
449 variability in growth rates during different phases of HT formation. Growth of the
450 differentiated cardiac tissue is relatively paused when the cc undergoes
451 morphogenesis to form the open HT during the second phase. This is consistent with
452 previous studies in mouse, chick and human models showing that proliferation drops
453 in the differentiated myocardium of the forming HT, while proliferation remains high
454 in the splanchnic mesoderm (Gert van den Berg et al. 2009, de Boer, B.A, 2012,
455 Sizarov et al. 2010). Our live analysis further showed that SHF cells do not contribute
456 to the forming HT during the differentiation pause, which correlates with the growth
457 rate reduction during this phase. This period coincides as well with the onset of
458 cardiac contractility in the embryo (Tyser et al. 2016).

459 Following the phase of differentiation pause, growth of the HT is reinitiated by
460 incorporation of new cells as the HT closes dorsally and the RV precursors are added
461 at the arterial pole during the third phase. During this third phase, similarities were
462 found in the differentiation dynamics of SHF precursors and splanchnic precursors
463 contributing to the dorsal regions of the linear HT. The dorsal aspect of the linear HT
464 gives rise to the inner curvature of the looped heart, which has an important
465 contribution to non-chamber myocardium, including atrio-ventricular canal and parts
466 of the conduction system (Christoffels et al., 2000). Our results suggest that the late
467 recruitment of progenitors to the dorsal HT could contribute to differences between
468 inner curvature cardiomyocytes and the rest of the heart tube.

469 While the live-imaging experiments were essential for the identification of the 5-7
470 hour hiatus between FHF and SHF differentiation, live imaging of the arterial pole
471 during the SHF differentiation phase was challenging and was complemented by 3D
472 reconstructions based on fixed and optically cleared embryos. These experiments

473 confirmed the pause in differentiation during open HT formation and its reactivation
474 during linear HT closure. In the future, it will be interesting to explore whether novel
475 non-toxic index-matching media compatible with embryo viability (Boothe et al.
476 2017) may alleviate the limitations for deep cardiac imaging during late HT formation.

477 Regarding the specification of FHF and SHF populations, previous prospective clonal
478 analyses showed that these lineages diverge around gastrulation (Devine et al., 2014;
479 Lescroart et al., 2014). In agreement with this, our tracking of cell lineages in the
480 cardiac forming region shows that sister cells share fates to either the cardiac crescent
481 or the SHF. In addition, the fact that cells contributing to the SHF do not differentiate
482 during the period when the cardiac crescent transforms into the primitive heart tube
483 may contribute to the establishment of the sharp boundary observed between left and
484 right ventricles later in development (Devine et al., 2014). Further studies will be
485 required to assess how this temporal pause of cardiac differentiation is regulated. The
486 molecular analyses of early FHF and SHF precursors suggest that intrinsic molecular
487 differences between the two lineages appear around or shortly after gastrulation
488 (Lescroart et al. 2014). These intrinsic differences may contribute to the regulation of
489 the two distinct differentiation schedules described here. These studies and our
490 observations, however, cannot discriminate whether this lineage allocation results
491 from intrinsic differences between these lineages or it is due to their exposure to
492 position-specific environments, especially as in our studies sister cells remain close
493 neighbors. Environmental cues thus could also control the sequential differentiation of
494 FHF and SHF precursors. The Wnt and BMP pathways are well known regulators of
495 cardiac differentiation (Ai et al., 2007; Jain et al., 2015; Klaus et al., 2007; Kwon et
496 al., 2007; Marvin et al., 2001; Qyang et al., 2007; Tirosh-Finkel et al., 2010; Ueno et
497 al., 2007) and specific mechanisms affecting these pathways could be operating
498 during the formation the HT, whereby the differentiation pathways could be
499 temporally restrained. Finally, the endoderm may also play a key role in mediating
500 FHF differentiation. Indeed cardiac mesoderm differentiation is affected in the
501 absence of Sox17 a transcription factor required for maintenance of the definitive
502 endoderm- and this is accompanied by the formation of a morphologically abnormal
503 HT (Pfister et al. 2011). It remains however unclear whether this effect is secondary
504 to an initial defect in foregut development that is observed in this mutant.

505 A recent study reported spontaneous calcium transients propagating laterally thought

506 the cardiac crescent (Tyser et al. 2016). Left/Right (L/R) asymmetry therefore exists
507 within the cardiac crescent, prior to any detectable cardiac contraction, and
508 BMP/SMAD1 signaling in the lateral plate mesoderm may be involved in this
509 asymmetry (Furtado et al. 2008). In our studies, however, we did not detect any L/R
510 difference in cTnnT expression by whole-mount immunodetection or Nkx2.5GFP
511 activation by live analysis in the cc.

512 Regarding the possible conservation of the temporal differentiation sequence
513 described here, elegant experiments in zebrafish using a cardiac myosin light chain
514 reporter line and a Kaede photo-conversion assay, addressed the temporal order of
515 cardiac differentiation in live embryos (de Pater et al., 2009; Liu and Stainier, 2012).
516 Two distinct phases of cardiomyocyte differentiation were also observed. During a
517 first phase, cardiomyocytes were recruited first into the ventricle and atria at the
518 venous pole. During a second phase, cardiomyocyte differentiation was observed at
519 the arterial pole of the HT. These pulse-chase experiments however do not address
520 whether cardiac differentiation is continuous or includes a differentiation-paused
521 phase, so further studies will be required to establish the conservation of the
522 observations made here for the mouse embryo.

523 Finally, an important question to address is the functional relevance of the three
524 distinct phases described here; more specifically, what is the role of the observed
525 differentiation pause. An interesting possibility is that this pause would be
526 functionally related to the extensive morphogenetic events that transform the cardiac
527 crescent into the HT. Our study demonstrates coordinated splanchnic mesoderm
528 movements during this phase. These movements involve a very active antero-medial
529 displacement of the splanchnic mesoderm surrounding the cc -mostly fated to the
530 SHF-. This behavior of the splanchnic mesoderm appears essential for transforming
531 the cc into a dorsally closed HT. Importantly, this displacement involves the sliding of
532 the splanchnic layer over the endoderm, suggesting an active role of SHF precursors
533 in this morphogenetic movement. Such displacement of the splanchnic mesoderm
534 over the endoderm during cardiogenesis had been suggested by classical time-lapse
535 studies in the chick embryo (de Haan, 1963) and it is tempting to speculate that a
536 similar phenomenon contributes to the incorporation of SHF cells to both poles of the
537 HT at later stages of HT development (van den Berg et al. 2009; Kelly RG, et al.
538 2001; Zaffran et al, 2004). These observations suggest that SHF cells do not represent

539 just a reservoir of cardiac precursors but play a morphogenetic role essential for heart
540 tube formation. The main consequence of the displacement of the splanchnic
541 mesoderm layer over the endoderm is the medial convergence of the left and right
542 frontiers between the cc and SHF to form the dorsal mesocardium and close the HT.
543 An important consequence of the differentiation pause described here is the stability
544 of the cc/SHF frontiers during these morphogenetic movements. This stability
545 prevents further spreading of the differentiation wave from the cc into the
546 SHF/splanchnic mesoderm, which could interfere the ability of the latter to efficiently
547 displace over the endoderm. We therefore hypothesize that the stability of the cc/SHF
548 frontiers –and thus the differentiation pause- would be essential to allow the effective
549 displacement of SHF/splanchnic mesoderm and elicit HT formation. The temporal
550 allocation of the morphogenetic phase after cc differentiation allows the formation of
551 the HT while simultaneously providing an incipient cardiac function essential for the
552 organization of embryonic circulation. This hypothesis poses a functional basis for the
553 alternation of differentiation and morphogenesis phases during HT formation.

554 Our study applies whole-embryo live analysis of cardiac development at tissue level
555 and with cellular resolution. We expect that extending this experimental approach will
556 allow to further uncover unexpected and novel mechanisms of organogenesis. While
557 limited attention had been paid so far to the temporal dynamics of differentiation
558 during embryonic development, this is an essential aspect of organogenesis
559 (Gogendeau et al., 2015; Parchem et al., 2015; Yang et al., 2015). Here we show the
560 relevance of differentiation timing regulation during heart tube formation and its
561 coordination with morphogenesis at the tissue level. Further understanding of the
562 molecular and cellular mechanisms underlying these phenomena will help us
563 expanding pools of cardiac progenitors in vitro or directing them towards
564 differentiation.

565

566 **MATERIALS AND METHODS**

567

568 **Mouse Strains:**

569 Mouse alleles used in the manuscript are listed including bibliographic references and
570 allele identities at the "Mouse Genome Informatics" data base (MGI,

571 http://www.informatics.jax.org/). *Mesp1*^{cre} (Saga et al., 1999, MGI:2176467), *Isl1*^{cre}
572 (Cai et al., 2003, MGI:3623159), *Nkx2.5*^{cre} (Stanley et al., 2002, MGI:2448972),
573 *Rosa26Rtdtomato* (Madisen et al., 2010, MGI:3809524), *Rosa26RmTmG* (Muzumdar
574 et al., 2007, MGI:3716464), *Nkx2.5eGFP* (Wu et al., 2006, MGI:5788423),
575 *Polr2a*^{CreERT2} (*RERT*) (Guerra et al., 2003, MGI:3772332) and *C57BL/6* (Charles
576 River). Mice were genotyped as previously described. All animal procedures were
577 approved by the CNIC Animal Experimentation Ethics Committee, by the
578 Community of Madrid (Ref. PROEX 220/15) and conformed to EU Directive
579 2010/63EU and Recommendation 2007/526/EC regarding the protection of animals
580 used for experimental and other scientific purposes, enforced in Spanish law under
581 Real Decreto 1201/2005.

582

583 **Immunostaining and Imaging:**

584 Embryos dissected in Dulbecco's modified Eagle's medium (DMEM, Invitrogen)
585 were fixed overnight in 2% PFA at 4C, then permeabilized in PBST (PBS containing
586 0.1% Triton X-100) and blocked (5% goat serum). Embryos were incubated overnight
587 at 4ºC with antibodies diluted in PBST: mouse anti-cTnnT (1:250, MS-295 Thermo
588 Scientific), rabbit anti-PH3 (1:250, 06-570 Millipore), CDC31 (553370 BD
589 Pharmingen™ clone MEC 13.3), SMA (C6198 Sigma) and rabbit anti-Laminin1
590 (1:500, Sigma, L9393). After washing in freshly prepared PBST at 4ºC, embryos
591 were incubated with secondary antibodies (Molecular Probes, A21121, A21141,
592 A11035) coupled to 488, 549 or 649 fluorophores as required at 1:250 and DAPI at
593 1:500 (Molecular Probes, D3571) overnight at 4ºC. Before imaging, embryos were
594 washed in PBST at room temperature and cleared with focus clear (Cell Explorer, FC-
595 101) to enhance the transparency of the embryo. Confocal images were obtained on a
596 SP8 Leica confocal microscope with a 20X oil objective (0.7 NA) at a 1024 × 1024
597 pixels dimension with a z-step of 2-4µm. Embryos were systematically imaged
598 throughout the entire heart tube from top to bottom.

599

600 **3D Reconstruction and Volumetric Measurement:**

601 For 3D rendering, fluorescent signal in confocal z-stacks was first segmented by
602 setting intensity thresholds using the trainable Weka segmentation tool plugin

603 available in Fiji (Arganda-Carreras et al., 2017; Schindelin et al., 2012). The resulting
604 z-stacks were then corrected manually on a slide-by-slide basis to eliminate
605 segmentation mistakes. In case of the cTnnT immunofluorescence images (Figure 1),
606 background signal from the yolk sack was manually masked. The volume of the
607 cTnnT positive myocardium was then computed by multiplying the total segmented
608 area by the z-stack interval using a custom Fiji macro. In the *Nkx2.5*$^{cre/+}$;
609 *Rosa26tdtomato*$^{+/-}$ and *Nkx2.5eGFP* embryos, fluorophore signal present in the
610 endothelium, endocardium and endoderm cells was manually masked prior to
611 segmentation (Figure 1A, Figure 1-figure supplement 1, Figure 2B, Figure 2-figure
612 supplement 2A,A' and, Figure 6A''). For 3D visualization of the 3D segmented
613 image stacks, Imaris software (Bitplane) was used.

614

615 **Embryo Culture and Two-photon Live-Imaging:**

616 Embryos were dissected at E7.5 in pre-equilibrated DMEM supplemented with 10%
617 foetal bovine serum, 25 mM HEPES-NaOH (pH 7.2), penicillin (50μml21) and
618 streptomycin (50mgml21). Embryos were staged on the basis of morphological
619 criteria (supplementary Figure 1) (Downs and Davies, 1993; Kirstie A. Lawson,
620 2016), and those between the bud and early somitogenesis stages were used for
621 culture and time-lapse imaging. To track the early phase of cardiac differentiation and
622 subsequent phases of morphogenesis, we used embryos at EHF to transversal HT
623 stage. Embryos were cultured in 50% fresh rat serum, 48% DMEM without phenol
624 red, 1% N-2 neuronal growth supplement (100X, Invitrogen 17502-048) and 1% B-27
625 supplement (50X Thermo Fisher Scientist 17504044) filter sterilised through a 0.2
626 mm filter. To hold embryos in position during time-lapse acquisition, we made
627 special plastic holders with holes of different diameters (0.5- 3 mm) to ensure a good
628 fit of embryos similarly to the traps developed by Nonaka et al. (Nonaka, 2009;
629 Nonaka et al., 2002). Embryos were mounted with their anterior side facing up. To
630 avoid evaporation, the medium was covered with mineral oil (Sigma-Aldrich; M8410).
631 Before starting the time-lapse acquisition, embryos were first pre-cultured for at least
632 2 hours in the microscopy culture set up. The morphology of the embryo was then
633 carefully monitored and if the embryos appeared unhealthy or rotate and move, they
634 were discarded, otherwise, time-lapse acquisition was performed. For the acquisition,
635 we used the Zeiss LSM780 equipped with a 5% CO2 incubator and a heating chamber

636 maintaining 37ºC. The objective lens used was a 20X(NA=1) dipping objective,
637 which allowed a long working distance for imaging mouse embryos and tissues. A
638 MaiTai laser line at 1000 nm was used for 2-channel 2-photon imaging. Acquisition
639 was done using Zen software (Zeiss). Typical image settings were: output power:
640 250mW, pixel dwell time: 7µs, line averaging: 2 and image dimension: 610x610µm
641 (1024x1024 pixels). To maximize the chance of covering the entire heart tube during
642 long-term time lapse videos, we allowed 150-200µm of free space between the
643 objective and the embryo at the beginning of the recording.

644

645 **Cell labeling, 3D tracking and GFP Intensity Measurement:**

646 For labeling single cells, tamoxifen was administered by oral gavage (2-4 mg/mL) in
647 *RERT;Rosa26R-tdtomato* (cell tracking) or *RERT;Rosa26RmTmG* mice (cell shape
648 study) at E7. Cell shape measurements were done on single cells, imaged in mosaic-
649 labeled, fixed and immunostained embryos and analyzed with Fiji software (Figure
650 2D, E). Tracking of tdtomato-labeled cells was done on single cells located within the
651 cardiogenic mesoderm -excluding endothelial, pericardial and endodermal cells- and
652 their GFP intensity was measured over time. To track cells manually in 4D stacks, the
653 MTrackJ Fiji plugin (Meijering et al., 2012) was used. A local square cursor (25x25
654 pixels) on the cell of interest snaps according to a bright centroid feature on a slice-
655 by-slice basis. Only tracks lasting for the entire length of the video were kept. When
656 an ambiguity arises in the tracking between consecutive time points, the track was
657 discarded. Tracks split at cell divisions. A cell division event is normally clearly
658 distinguishable over at least 2 time points. In case one of the two daughter cells is not
659 tractable, the other daughter cell is still tracked. Each track is assigned an ID number
660 and excel files with all the tracks coordinates in x, y, z and t was generated.
661 Coordinates of each track were converted into 8-bit 4D images using a custom Fiji
662 macro in which each cell was represented by a sphere of specific pixel intensity, from
663 1 to 255, while pixels corresponding to background were set to zero. The 4D images
664 were then opened with Imaris to perform visualization of the 3D trajectories of each
665 cell using the "spots" tool, where each object were identified according to pixel
666 intensity. GFP intensity measurement is performed by segmentation of cell shape. A
667 Gaussian filter whose radius is adjusted to the typical size of a cell was first applied,
668 followed by a Laplacian filter. The resulting 32 bits image was next converted to a

669 mask by thresholding. When objects touched each other, a watershed on the binary
670 mask and manual corrections was applied. Each segmented cell was checked and
671 tracked manually for accuracy. In Figure 3B' nuclei segmentation was performed
672 manually. The mean GFP signal intensity of the segmented objects was then
673 measured using the "analyze particle" tool in Fiji. To quantify the GFP level of
674 tracked cells through time, four to five successive time points were arbitrarily chosen
675 in each video (Figure 5F, Figure 6C, D and Figure 5-figure supplement 1C) except in
676 Figure 5D and Figure 6I, where GFP intensity level was measured in every time point.
677 Background intensities were measured in neural tube cells, which are known to be
678 negative for GFP and cTnnT. Tables containing ID number of tracked cells and GFP
679 intensities were generated and plotted using Prism statistical software.

680

681 **Statistical Analysis:**

682 For comparisons of two groups, a Man-Whitney U-test was used using Prism
683 statistical software. To find a correlation between GFP and cTnnT levels of 0.8 with
684 an alpha-level f 0.05 and a power of 0.2 at least 10 cells per embryo were required
685 (Figure 3D and Figure 3-figure supplement 2C). Many more cells were computed for
686 each experiment. The linear fit was done using "lm" function from R statistical
687 software (https://www.r-project.org/). To calculate the average speed of splanchnic
688 mesoderm displacement, the shortest distance between the left and right splanchnic
689 mesoderm was calculated in two z-level, using the measure tool in Fiji, and the
690 variation in this distance by time unit was divided by 2, to determine the speed of
691 movement of each sliding side of the splanchnic mesoderm.

692

693 **Acknowledgments**

694 We thank the CNIC Microscopy unit for help with the live confocal analysis, Fatima
695 Sanchez Cabo for help with the statistical analyses and Florencia Cavodeassi, Miguel
696 Manzanares, Briane Laruy and members of the Torres lab for helpful comments on
697 the manuscript. This work was supported by grants BFU2015-71519-P, BFU2015-
698 70193-REDT and RD16/0011/0019 (ISCIII) from the Spanish Ministry of Economy,
699 Industry and Competitiveness (MEIC). KI was supported by a Human Frontiers
700 Science Program (LT000609/2015) and EMBO (ATL1275-2014) postdoctoral

fellowships. The CNIC is supported by the Spanish MEIC and the Pro CNIC Foundation, and is a Severo Ochoa Center of Excellence (MINECO award SEV-2015-0505). The authors declare no conflicts of interest.

REFERENCES:

Abu-Issa, R. (2014). Heart fields: spatial polarity and temporal dynamics. Anat Rec (Hoboken) 297, 175-182.

Abu-Issa, R., Waldo, K., and Kirby, M.L. (2004). Heart fields: one, two or more? Dev Biol 272, 281-285.

Ai, D., Fu, X., Wang, J., Lu, M.F., Chen, L., Baldini, A., Klein, W.H., and Martin, J.F. (2007). Canonical Wnt signaling functions in second heart field to promote right ventricular growth. Proc Natl Acad Sci U S A 104, 9319-9324.

Arganda-Carreras, I., Kaynig, V., Rueden, C., Eliceiri, K.W., Schindelin, J., Cardona, A., and Seung, H.S. (2017). Trainable Weka Segmentation: a machine learning tool for microscopy pixel classification. Bioinformatics.

Biben, C., Weber, R., Kesteven, S., Stanley, E., McDonald, L., Elliott, D.A., Barnett, L., Koentgen, F., Robb, L., Feneley, M., et al. (2000). Cardiac septal and valvular dysmorphogenesis in mice heterozygous for mutations in the homeobox gene Nkx2-5. Circ Res 87, 888-895.

Brade, T., Gessert, S., Kuhl, M., and Pandur, P. (2007). The amphibian second heart field: Xenopus islet-1 is required for cardiovascular development. Dev Biol 311, 297-310.

Buckingham, M., Meilhac, S., and Zaffran, S. (2005). Building the mammalian heart from two sources of myocardial cells. Nat Rev Genet 6, 826-835.

Cai, C.L., Liang, X., Shi, Y., Chu, P.H., Pfaff, S.L., Chen, J., and Evans, S. (2003). Isl1 identifies a cardiac progenitor population that proliferates prior to differentiation and contributes a majority of cells to the heart. Dev Cell 5, 877-889.

Chen, C.M., Miranda, A.M., Bub, G., and Srinivas, S. (2014). Detecting cardiac contractile activity in the early mouse embryo using multiple modalities. Front Physiol 5, 508.

Christoffels, V.M., Habets, P.E., Franco, D., Campione, M., de Jong, F., Lamers, W.H., Bao, Z.Z., Palmer, S., Biben, C., Harvey, R.P., et al. (2000). Chamber formation and morphogenesis in the developing mammalian heart. Dev Biol 223, 266-278.

Christoffels, V.M., Mommersteeg, M.T., Trowe, M.O., Prall, O.W., de Gier-de Vries,

C., Soufan, A.T., Bussen, M., Schuster-Gossler, K., Harvey, R.P., Moorman, A.F., et al. (2006). Formation of the venous pole of the heart from an Nkx2-5-negative precursor population requires Tbx18. Circ Res 98, 1555-1563.

de Boer, B.A., van den Berg, G., de Boer, P.A., Moorman, A.F., and Ruijter, J.M. (2012). Growth of the developing mouse heart: an interactive qualitative and quantitative 3D atlas. Dev Biol 368, 203-213.

de Hann RL. (1963) Migration patterns of the precardiac mesoderm in the early chick embryo. Exp Cell Res.;29:544-60.

de Pater, E., Clijsters, L., Marques, S.R., Lin, Y.F., Garavito-Aguilar, Z.V., Yelon, D., and Bakkers, J. (2009). Distinct phases of cardiomyocyte differentiation regulate growth of the zebrafish heart. Development 136, 1633-1641.

Devine, W.P., Wythe, J.D., George, M., Koshiba-Takeuchi, K., and Bruneau, B.G. (2014). Early patterning and specification of cardiac progenitors in gastrulating mesoderm. eLife 2014;3:e03848

Diogo, R., Kelly, R.G., Christiaen, L., Levine, M., Ziermann, J.M., Molnar, J.L., Noden, D.M., and Tzahor, E. (2015). A new heart for a new head in vertebrate cardiopharyngeal evolution. Nature *520*, 466-473.

Downs, K.M., and Davies, T. (1993). Staging of gastrulating mouse embryos by morphological landmarks in the dissecting microscope. Development 118, 1255-1266.

Evans, S.M., Yelon, D., Conlon, F.L., and Kirby, M.L. (2010). Myocardial lineage development. Circ Res 107, 1428-1444.

Francou, A., Saint-Michel, E., Mesbah, K., and Kelly, R.G. (2014). TBX1 regulates epithelial polarity and dynamic basal filopodia in the second heart field. Development 141, 4320-4331.

Furtado MB, Solloway MJ, Jones VJ, Costa MW, Biben C, Wolstein O, Preis JI, Sparrow DB, Saga Y, Dunwoodie SL, Robertson EJ, Tam PP, Harvey RP. (2008) BMP/SMAD1 signaling sets a threshold for the left/right pathway in lateral plate mesoderm and limits availability of SMAD4 Genes Dev. Nov 1;22(21):3037-49.

Galli D, Domínguez JN, Zaffran S, Munk A, Brown NA, Buckingham ME. Atrial myocardium derives from the posterior region of the second heart field, which acquires left-right identity as Pitx2c is expressed. Development. 2008 Mar;135(6):1157-67.

Gogendeau, D., Siudeja, K., Gambarotto, D., Pennetier, C., Bardin, A.J., and Basto, R. (2015). Aneuploidy causes premature differentiation of neural and intestinal stem cells. Nat Commun 6, 8894.

Guerra, C., Mijimolle, N., Dhawahir, A., Dubus, P., Barradas, M., Serrano, M., Campuzano, V., and Barbacid, M. (2003). Tumor induction by an endogenous K-ras oncogene is highly dependent on cellular context. Cancer Cell 4, 111-120.

797
798 Jain, R., Li, D., Gupta, M., Manderfield, L.J., Ifkovits, J.L., Wang, Q., Liu, F., Liu, Y.,
799 Poleshko, A., Padmanabhan, A., et al. (2015). Integration of Bmp and Wnt signaling
800 by Hopx specifies commitment of cardiomyoblasts. Science 348, aaa6071.
801
802 Kelly, R.G., Brown, N.A., and Buckingham, M.E. (2001). The arterial pole of the
803 mouse heart forms from Fgf10-expressing cells in pharyngeal mesoderm. Dev Cell 1,
804 435-440.
805
806 Kelly, R.G., Buckingham, M.E., and Moorman, A.F. (2014). Heart fields and cardiac
807 morphogenesis. Cold Spring Harb Perspect Med 4.
808
809 Kirstie A. Lawson, V.W. (2016). A Revised Staging of Mouse Development Before
810 Organogenesis. Kaufman's Atlas of Mouse Development Supplement.
811
812 Klaus, A., Saga, Y., Taketo, M.M., Tzahor, E., and Birchmeier, W. (2007). Distinct
813 roles of Wnt/beta-catenin and Bmp signaling during early cardiogenesis. Proc Natl
814 Acad Sci U S A 104, 18531-18536.
815
816 Kwon, C., Arnold, J., Hsiao, E.C., Taketo, M.M., Conklin, B.R., and Srivastava, D.
817 (2007). Canonical Wnt signaling is a positive regulator of mammalian cardiac
818 progenitors. Proc Natl Acad Sci U S A 104, 10894-10899.
819
820 Laugwitz, K.L., Moretti, A., Lam, J., Gruber, P., Chen, Y., Woodard, S., Lin, L.Z.,
821 Cai, C.L., Lu, M.M., Reth, M., et al. (2005). Postnatal isl1+ cardioblasts enter fully
822 differentiated cardiomyocyte lineages. Nature 433, 647-653.
823
824 Lescroart, F., Chabab, S., Lin, X., Rulands, S., Paulissen, C., Rodolosse, A., Auer, H.,
825 Achouri, Y., Dubois, C., Bondue, A., et al. (2014). Early lineage restriction in
826 temporally distinct populations of Mesp1 progenitors during mammalian heart
827 development. Nat Cell Biol 16, 829-840.
828
829 Lescroart, F., Hamou, W., Francou, A., Theveniau-Ruissy, M., Kelly, R.G., and
830 Buckingham, M. (2015). Clonal analysis reveals a common origin between
831 nonsomite-derived neck muscles and heart myocardium. Proc Natl Acad Sci U S A
832 *112*, 1446-1451.
833
834 Lescroart, F., Kelly, R.G., Le Garrec, J.F., Nicolas, J.F., Meilhac, S.M., and
835 Buckingham, M. (2010). Clonal analysis reveals common lineage relationships
836 between head muscles and second heart field derivatives in the mouse embryo.
837 Development *137*, 3269-3279.
838
839 Lien, C.L., Wu, C., Mercer, B., Webb, R., Richardson, J.A., and Olson, E.N. (1999).
840 Control of early cardiac-specific transcription of Nkx2-5 by a GATA-dependent
841 enhancer. Development 126, 75-84.
842
843 Linask, K.K., Knudsen, K.A., and Gui, Y.H. (1997). N-cadherin-catenin interaction:
844 necessary component of cardiac cell compartmentalization during early vertebrate
845 heart development. Dev Biol 185, 148-164.
846

847 Liu, J., and Stainier, D.Y. (2012). Zebrafish in the study of early cardiac development.
848 Circ Res 110, 870-874.
849
850 Ma, Q., Zhou, B., and Pu, W.T. (2008). Reassessment of Isl1 and Nkx2-5 cardiac fate
851 maps using a Gata4-based reporter of Cre activity. Dev Biol 323, 98-104.
852
853 Madisen, L., Zwingman, T.A., Sunkin, S.M., Oh, S.W., Zariwala, H.A., Gu, H., Ng,
854 L.L., Palmiter, R.D., Hawrylycz, M.J., Jones, A.R., et al. (2010). A robust and high-
855 throughput Cre reporting and characterization system for the whole mouse brain. Nat
856 Neurosci 13, 133-140.
857
858 Marvin, M.J., Di Rocco, G., Gardiner, A., Bush, S.M., and Lassar, A.B. (2001).
859 Inhibition of Wnt activity induces heart formation from posterior mesoderm. Genes
860 Dev 15, 316-327.
861
862 Meijering, E., Dzyubachyk, O., and Smal, I. (2012). Methods for cell and particle
863 tracking. Methods Enzymol 504, 183-200.
864
865 Meilhac, S.M., Esner, M., Kelly, R.G., Nicolas, J.F., and Buckingham, M.E. (2004a).
866 The clonal origin of myocardial cells in different regions of the embryonic mouse
867 heart. Dev Cell 6, 685-698.
868
869 Meilhac, S.M., Esner, M., Kerszberg, M., Moss, J.E., and Buckingham, M.E. (2004b).
870 Oriented clonal cell growth in the developing mouse myocardium underlies cardiac
871 morphogenesis. J Cell Biol 164, 97-109.
872
873 Mjaatvedt, C.H., Nakaoka, T., Moreno-Rodriguez, R., Norris, R.A., Kern, M.J.,
874 Eisenberg, C.A., Turner, D., and Markwald, R.R. (2001). The outflow tract of the
875 heart is recruited from a novel heart-forming field. Dev Biol 238, 97-109.
876
877 Moorman, A.F., Christoffels, V.M., Anderson, R.H., and van den Hoff, M.J. (2007).
878 The heart-forming fields: one or multiple? Philos Trans R Soc Lond B Biol Sci 362,
879 1257-1265.
880
881 Moretti, A., Caron, L., Nakano, A., Lam, J.T., Bernshausen, A., Chen, Y., Qyang,
882 Y.,Bu, L., Sasaki, M., Martin-Puig, S., et al. (2006). Multipotent embryonic isl1+
883 progenitor cells lead to cardiac, smooth muscle, and endothelial cell diversification.
884 Cell 127, 1151-1165.
885
886 Muzumdar, M.D., Tasic, B., Miyamichi, K., Li, L., and Luo, L. (2007). A global
887 double-fluorescent Cre reporter mouse. Genesis 45, 593-605.
888
889 Nonaka, S. (2009). Modification of mouse nodal flow by applying artificial flow.
890 Methods Cell Biol 91, 287-297.
891
892 Nonaka, S., Shiratori, H., Saijoh, Y., and Hamada, H. (2002). Determination of left-
893 right patterning of the mouse embryo by artificial nodal flow. Nature 418, 96-99.
894
895 Parchem, R.J., Moore, N., Fish, J.L., Parchem, J.G., Braga, T.T., Shenoy, A., Oldham,
896 M.C., Rubenstein, J.L., Schneider, R.A., and Blelloch, R. (2015). miR-302 Is

897 Required for Timing of Neural Differentiation, Neural Tube Closure, and Embryonic
898 Viability. Cell Rep 12, 760-773.
899
900 Pfister S1, Jones VJ, Power M, Truisi GL, Khoo PL, Steiner KA, Kanai-Azuma M,
901 Kanai Y, Tam PP, Loebel DA. (2011) Sox17-dependent gene expression and early
902 heart and gut development in Sox17-deficient mouse embryos. Int J Dev
903 Biol.;55(1):45-58
904
905 Prall, O.W., Menon, M.K., Solloway, M.J., Watanabe, Y., Zaffran, S., Bajolle, F.,
906 Biben, C., McBride, J.J., Robertson, B.R., Chaulet, H., et al. (2007). An Nkx2-
907 5/Bmp2/Smad1 negative feedback loop controls heart progenitor specification and
908 proliferation. Cell 128, 947-959.
909
910 Qyang, Y., Martin-Puig, S., Chiravuri, M., Chen, S., Xu, H., Bu, L., Jiang, X., Lin, L.,
911 Granger, A., Moretti, A., et al. (2007). The renewal and differentiation of Isl1+
912 cardiovascular progenitors are controlled by a Wnt/beta-catenin pathway. Cell Stem
913 Cell 1, 165-179.
914
915 Ramsbottom, S.A., Sharma, V., Rhee, H.J., Eley, L., Phillips, H.M., Rigby, H.F.,
916 Dean, C., Chaudhry, B., and Henderson, D.J. (2014). Vangl2-regulated polarisation of
917 second heart field-derived cells is required for outflow tract lengthening during
918 cardiac development. PLoS Genet 10, e1004871.
919
920 Saga, Y., Hata, N., Kobayashi, S., Magnuson, T., Seldin, M.F., and Taketo, M.M.
921 (1996). MesP1: a novel basic helix-loop-helix protein expressed in the nascent
922 mesodermal cells during mouse gastrulation. Development 122, 2769-2778.
923
924 Saga, Y., Miyagawa-Tomita, S., Takagi, A., Kitajima, S., Miyazaki, J., and Inoue, T.
925 (1999). MesP1 is expressed in the heart precursor cells and required for the formation
926 of a single heart tube. Development 126, 3437-3447.
927
928 Schindelin, J., Arganda-Carreras, I., Frise, E., Kaynig, V., Longair, M., Pietzsch, T.,
929 Preibisch, S., Rueden, C., Saalfeld, S., Schmid, B., et al. (2012). Fiji: an open-source
930 platform for biological-image analysis. Nat Methods 9, 676-682.
931
932 Sinha, T., Wang, B., Evans, S., Wynshaw-Boris, A., and Wang, J. (2012). Disheveled
933 mediated planar cell polarity signaling is required in the second heart field lineage for
934 outflow tract morphogenesis. Dev Biol 370, 135-144.
935 Formation of the building plan of the human heart: morphogenesis, growth, and
936 differentiation. (2011) Sizarov A, Ya J, de Boer BA, Lamers WH, Christoffels VM,
937 Moorman AF. Circulation.;123(10):1125-35.
938
939 Spater, D., Abramczuk, M.K., Buac, K., Zangi, L., Stachel, M.W., Clarke, J., Sahara,
940 M., Ludwig, A., and Chien, K.R. (2013). A HCN4+ cardiomyogenic progenitor
941 derived from the first heart field and human pluripotent stem cells. Nat Cell Biol 15,
942 1098-1106.
943
944 Stanley, E.G., Biben, C., Elefanty, A., Barnett, L., Koentgen, F., Robb, L., and
945 Harvey, R.P. (2002). Efficient Cre-mediated deletion in cardiac progenitor cells
946 conferred by a 3'UTR-ires-Cre allele of the homeobox gene Nkx2-5. Int J Dev Biol 46,

947 431-439.
948
949 Tirosh-Finkel, L., Zeisel, A., Brodt-Ivenshitz, M., Shamai, A., Yao, Z., Seger, R.,
950 Domany, E., and Tzahor, E. (2010). BMP-mediated inhibition of FGF signaling
951 promotes cardiomyocyte differentiation of anterior heart field progenitors.
952 Development 137, 2989-3000.
953
954 Tyser, R.C., Miranda, A.M., Chen, C.M., Davidson, S.M., Srinivas, S., and Riley, P.R.
955 (2016). Calcium handling precedes cardiac differentiation to initiate the first heartbeat.
956 Elife 5.
957
958 Ueno, S., Weidinger, G., Osugi, T., Kohn, A.D., Golob, J.L., Pabon, L., Reinecke, H.,
959 Moon, R.T., and Murry, C.E. (2007). Biphasic role for Wnt/beta-catenin signaling in
960 cardiac specification in zebrafish and embryonic stem cells. Proc Natl Acad Sci U S A
961 104, 9685-9690.
962
963 van den Berg G, Abu-Issa R, de Boer BA, Hutson MR, de Boer PA, Soufan AT,
964 Ruijter JM, Kirby ML, van den Hoff MJ, Moorman AF. (2009) A caudal proliferating
965 growth center contributes to both poles of the forming heart tube. Circ Res.
966 104(2):179-88.
967
968 Waldo, K.L., Kumiski, D.H., Wallis, K.T., Stadt, H.A., Hutson, M.R., Platt, D.H., and
969 Kirby, M.L. (2001). Conotruncal myocardium arises from a secondary heart field.
970 Development 128, 3179-3188.
971
972 Wu, S.M., Fujiwara, Y., Cibulsky, S.M., Clapham, D.E., Lien, C.L., Schultheiss, T.M.,
973 and Orkin, S.H. (2006). Developmental origin of a bipotential myocardial and smooth
974 muscle cell precursor in the mammalian heart. Cell 127, 1137-1150.
975
976 Yang, S.L., Yang, M., Herrlinger, S., Liang, C., Lai, F., and Chen, J.F. (2015). MiR-
977 302/367 regulate neural progenitor proliferation, differentiation timing, and survival
978 in neurulation. Dev Biol 408, 140-150.
979
980 Yuan, S., and Schoenwolf, G.C. (2000). Islet-1 marks the early heart rudiments and is
981 asymmetrically expressed during early rotation of the foregut in the chick embryo.
982 Anat Rec 260, 204-207.
983
984 Zaffran, S., Kelly, R.G., Meilhac, S.M., Buckingham, M.E., and Brown, N.A. (2004).
985 Right ventricular myocardium derives from the anterior heart field. Circ Res 95, 261-
986 268.
987

988 **FIGURE LEGENDS:**

989

990 **Figure 1. Overview of HT morphogenesis and growth.**

991 (A) Frontal view of an *Nkx2.5*$^{cre/+}$; *Rosa26Rtdtomato* embryo at EHF stage. (A') 3D
992 reconstruction of the tdtomato signal in the cardiogenic area. Signal from tdtomato+
993 endothelial cells identified by shape was manually masked. See also Video 1. (B-G)
994 Immunostaining for cTnnT (red) and Dapi (blue) showing six consecutive stages
995 during cardiac differentiation (B-D) and HT morphogenesis (E-G). (B) At EHF cTnnt
996 is initially not detectable. (C-D) During early somitogenesis, cTnnT signal becomes
997 detectable in the cc. Insets in (B-D): magnification of single optical sections showing
998 cTnnT localization and cell shape. (C'-G' and E''-G'') Corresponding 3D renderings
999 from cTnnT signal reconstruction. Red arrows in (E'-G') highlight the dorsal closure
1000 of the HT. Yellow arrow in G'' highlights the arterial pole (prospective RV). See also
1001 Video 2. (H) Quantification of the arterial pole/RV length in the open HT (41.4
1002 ±14.0μm, n=5) and after dorsal closure (109 ±43.44μm, n=7), mean ± SD, p=0.0025.
1003 (I) Quantification of the cardiac volume at the different stages of HT development.
1004 (Initial cc: 1.63.106μm3 ± 0.13, n=4, cc: 2.89.106 ± 0.37μm3, n=3, transversal HT:
1005 3.367. 106μm3 ± 0.95, n=5, open HT: 4.29.106μm3 ± 1.08, n=6, linear HT: 6.37.
1006 106μm3 ± 1.01, n=5, mean ± SD). P-values are indicated on the graph. (J)
1007 Immunostaining of an *Nkx2.5eGFP* embryo for PH3 (red) and Dapi (blue) at HT
1008 stage, showing proliferative cells in the ventricle. Scale bars: 100μm

1009

1010 **Figure 1-figure supplement 1. Criteria for embryo staging**

1011 We determined the developmental stage of embryos based on morphological
1012 landmarks (Downs and Davies, 1993; Kirstie A. Lawson, 2016). (A) At bud stage/E7,
1013 a small allantois bud is visible. At neural plate stage/E7.5, the allantois is larger and
1014 projects into the yolk sack cavity. The anterior neuroectoderm is enlarged. (B) At
1015 EHF/E7.5, the neural plate starts to form the head fold. During somitogenesis, a
1016 clearly visible foregut pocket appears and the head folds are located dorsally and
1017 anteriorly to the cardiac primordium. The cc has differentiated. It transforms
1018 successively into the transversal HT, the open HT and the linear HT closed dorsally
1019 and with a prominent arterial pole/RV. Scale bars: 100μm.

1020

1021 **Figure 1-figure supplement 2. Lineage tracing using the *Nkx2.5*^{cre} driver shows a**

1022 **contribution of labeled cells to the cardiogenic regions but not to the endoderm**
1023 **at EHF stage**
1024 (A, A') *Nkx2.5*$^{cre/+}$ *; Rosa26Rtdtomato*$^{+/-}$ embryo at EHF stage (same embryo as in
1025 Figure 1A. Here a single optical section is shown). Tdtomato labeling is detected in
1026 the cardiac progenitors, endothelial (yellow arrow) and endocardial cells (green
1027 arrows). No labeling is detected in the endoderm (gray arrow). (A'') Segmentation of
1028 cardiac crescent progenitors (shown in dark green) used for the 3D reconstruction
1029 shown in Figure 1A' overlaid with the raw image and. Scale bars: 100μm
1030
1031 **Figure 1-figure supplement 3. Faint cTnnT signal starts to be detected at EHF**
1032 **stage in apico-basally polarized cc cells.**
1033 (A) A *Mesp1*$^{cre/+}$*; Rosa26Rtdtomato*$^{+/-}$ embryo at EHF stage showing mesodermal
1034 labeling (green)- immunostaining against cTnnT (red) and Dapi (blue). Note that the
1035 embryo is at a slightly more advanced developmental stage than those shown in
1036 (Figure 1B) because the foregut pocket is more invaginated. (A') White inset in (A).
1037 Faint cTnnT signal (red) in few mesodermal cells (arrows) can be detected. (B-B')
1038 *Mesp1*$^{cre/+}$*; Rosa26Rtdtomato*$^{+/-}$ embryo showing the mesoderm in red and
1039 immunostained against the tight junction component zona-occludens-1 (ZO-1) (green)
1040 and Dapi (blue). The cc cells (as seen in transversal sections) have an AB polarized
1041 epithelial morphology. fg: foregut, endo: endoderm, endoc: endocardium. Scale bars:
1042 150μm.
1043
1044 Figure Source Data 1
1045 Source data for Figure 1H and I
1046
1047 **Figure 2. Visualization of the boundary between FHF and SHF.**
1048 (A-A'') An *Nkx2.5*$^{cre/+}$ *; Rosa26Rtdtomato*$^{+/-}$ embryo immunostained for cTnnT
1049 (green) and Dapi (blue) showing cells of the Nkx2.5+ lineage populating both the
1050 FHF and SHF. (A' and A'') Cross-sections in xz along the dotted lines 1 and 2 shown
1051 in (A), and corresponding schematics highlighting the endoderm (blue), FHF (green),
1052 SHF (red) and endocardium (yellow). Note that tdtomato signal is also detected in the
1053 endoderm and endocardium. (B) 3D reconstruction of the FHF (green) and SHF (red);
1054 (B') 3D drawing of the border between the FHF and SHF (in red) and the FHF and

1055 yolk sack (in green) (based on the embryo shown in (A). For SHF rendering, the
1056 tdtomato+ splanchnic mesoderm was depicted. The FHF was rendered using the
1057 cTnnT signal. See also Video 3. (C) Quantification of the cell roundness (rnd) index
1058 of cardiomyocytes at HT stage on single optical sections. Black bars indicate mean.
1059 Rnd index for cTnnT+ (green) cells is 0.71 ± 0.16 and for cTnnT- (red) cells is 0.38 ±
1060 0.16, mean ± SD, exact p value < 0.0001. (D-E) Membrane-GFP labeling of typical
1061 cTnnT+ FHF (D) and cTnnT-SHF (E) cells at longitudinal HT stage. The specimen is
1062 immunostained for cTnnT (blue), the basement membrane marker Laminin1 (red) and
1063 GFP (green). (F) Single optical section of the same embryo shown in (A, B). (F'-F''')
1064 Inset: red arrows point to cells localizing weak cTnnT signal and have columnar cell
1065 shape in the SHF. White arrows point to cTnnT-negative SHF cells. splan. meso:
1066 splanchnic mesoderm, endo: endoderm, fg: foregut. In all the embryos immunostained
1067 for cTnnT, the yolk sack signal is non-specific background (indicated by an asterisks).
1068 Scale bars: 100μm except in (D-E): 50μm
1069
1070 **Figure 2- figure supplement 1. Image segmentation of the FHF and SHF.**
1071 (A) Single optical section of an *Nkx2.5*$^{cre/+}$*; Rosa26Rtdtomato*$^{+/-}$ embryo
1072 immunostained for cTnnT (green) and Dapi (blue). Gray arrows highlight tdtomato
1073 signal in the endoderm (A') Segmentation of the FHF and SHF. Segmentation of the
1074 FHF (green) is based on the cTnnT signal while the segmentation of the SHF is based
1075 on the tdtomato positive and cTnnT negative signal (in red). tdtomato labeling in the
1076 endoderm and endocardium has been removed manually.
1077
1078 **Figure 2- figure supplement 2. Endocardium localization in the cardiac crescent.**
1079 (A) Maximum z-projection and (B, B') single optical section of an embryo
1080 immunostained for smooth muscle actin (SMA, labeling differentiated
1081 cardiomyocytes) (red), CD31 (labeling the endocardium) (green) and ZO-1 (blue).
1082 endo: endoderm, splan. meso: splanchnic mesoderm Scale bars: 150μm.
1083
1084 Figure Source Data 2
1085 Source data for Figure 2C
1086

1087 **Figure 3. The *Nkx2.5eGFP* transgene is robustly expressed in cTnnT-positive**
1088 **cardiomyocytes**
1089 (A) z-maximum projection of an *Nkx2.5eGFP* embryo at transversal HT stage
1090 immunostained for cTnnT (red) and Dapi (blue) showing high GFP level in
1091 differentiated cardiomyocytes. (B) Single optical section of an *Nkx2.5eGFP* embryo
1092 at transversal HT stage immunostained for cTnnT (red) and Dapi (blue). (B') Inset in
1093 (B): arrow points the transition between cTnnT+ and cTnnT- domains, corresponding
1094 to FHF and SHF, respectively. Dotted line represents the linescan measured in (D) (C)
1095 Example of manual segmentation based on Dapi nuclei in cells located in the
1096 splanchnic mesoderm and in the neural tube. (D) Linear mixed-effects model to find
1097 the relationship between the background-substracted GFP and cTnnT levels adjusted
1098 by embryo (GFP=0.95*cTnnT). (E) GFP and cTnnT mean intensities measured
1099 within manually segmented cells along the boundary from SHF to cTnnT-positive
1100 FHF (B') (n=130 cells analysed in 4 independent embryos). Scale bar: 100µm
1101
1102 **Figure 3- figure supplement 1. The *Nkx2.5eGFP* and cTnnT labeling at different**
1103 **z-levels.**
1104 (A) z-maximum projection and yz view of a *Nkx2.5eGFP* embryo immunostained
1105 against cTnnT showing overlap between eGFP signal and cTnnT localisation along
1106 the z dimension. (B) z-maximum projection and optical sections at different z-level of
1107 an *Nkx2.5eGFP* embryo, immunostained for cTnnT (red) and Dapi (blue), showing
1108 overlapping expression of GFP and cTnnT signal. Scale bar: 100µm
1109
1110 **Figure 3- figure supplement 2. High GFP levels are detected in strongly labeled**
1111 **cTnnT cells.**
1112 (A,B) Normalized GFP and cTnnT mean level for single segmented cell. Each dot
1113 represents a single segmented cell (A) located in the FHF and SHF and (B) located at
1114 the boundary zone between the FHF and SHF (n=130 cells analyzed from 8 embryos).
1115 (C) Linear mixed-effects model to find the relationship between the background
1116 substracted GFP and cTnnT levels adjusted by embryo for cell located at the
1117 boundary between the FHF and SHF (GFP=0.94*cTnnT, R2=0.77, p<2.2e-16). Cells
1118 are being considered positive for cTnnT when their mean intensity value is above 0.
1119 Note that small GFP signal can be detected in the cTnnT-negative SHF cells.

1120

1121 **Figure 3- figure supplement 3. *Nkx2.5Cre* genetic tracing labels both the FHF**
1122 **and SHF**

1123 (**A**) The GFP expression of the *Nkx2.5eGFP* reporter does not fully overlap with
1124 tdtomato expression pattern in *Nkx2.5*$^{cre/+}$*; Rosa26Rtdtomato*$^{+/-}$*; Nkx2.5eGFP* embryos
1125 at the level of the splanchnic mesoderm/SHF. Scale bar: 100µm.

1126

1127 Figure Source Data 3

1128 Source data for Figure 3D and E

1129

1130

1131 **Figure 4. Live-imaging of cardiac differentiation and morphogenesis**

1132 (A) Schematic of the set up for imaging live mouse embryos from EHF up to
1133 completion of HT formation. (B) Parameters xyzt during live-imaging. (C) An
1134 embryonic holder maintains the embryo still during live-imaging. (D-E) After over 10
1135 hours of ex-vivo culture inside the two-photon chamber, the embryo has grown and
1136 the cardiac crescent has transformed into a beating heart tube. Arrows in (E) point to
1137 the deformation of the heart ventricle due to heart beats. See also Video 4. (F-F'')
1138 Time-lapse video sequence of a *Mesp1*$^{cre/+}$*; Rosa26Rtdtomato*$^{+/-}$ embryo –reporting
1139 anterior mesoderm–, showing the transition from cardiac crescent stage to heart tube
1140 stage. Note that at the initial time point, the foregut pocket is already visible. Arrows
1141 indicate the major tissue movements visible (folding of the cardiac crescent, medial
1142 movement of the splanchnic mesoderm). The differentiation of cardiomyocytes
1143 detaching from the endoderm is visible in (F'). White arrows point to the
1144 endocardium. The formation of the endocardial lumen in the transversal HT is visible
1145 in F'. By 8h35m, the open HT is fully formed and beating regularly. Yellow lines
1146 represent distances between the left and right splanchnic mesoderm. Images are z-
1147 max projection of 84 sections covering 180µm (F) and 9 sections covering 36µm (F')
1148 acquired every 4µm. See also Videos 5-6. (G-G'') Time-lapse video of an *Nkx2.5*$^{cre/+}$*;*
1149 *Rosa26RmT/mG*$^{+/-}$ embryo during the early stages of cardiac differentiation. Images
1150 are z-max projection of 87 sections acquired every 5µm covering 437µm. (G') shows
1151 in a single optical section how progenitors change in cell shape and move away from
1152 the endoderm during differentiation towards cardiomyocytes (from inset in (G)). (G'')

1153 Cartoon depicting the change in cell shape taking place during cardiac differentiation.
1154 See also Video 7. (H) Time-lapse video sequences of *Nkx2.5eGFP* embryos from
1155 transversal HT showing low GFP level prior to cardiomyocyte differentiation and
1156 increase in GFP intensity level during the stages cardiomyocytes undergo
1157 differentiation. (H' and H''), cardiomyocytes in single magnified optical sections.
1158 Images are z-maximum projections of 70 sections acquired every 6µm covering
1159 420µm. See also Videos 10. (I) Estimate of the timing between different heart tube
1160 development stages. fg: foregut cc: cardiac crescent, endoc: endocardium, ao: aorta,
1161 endo: endoderm. Scale bars: 100µm.
1162
1163
1164 **Figure 4- figure supplement 1. Embryos can be cultured and imaged under the**
1165 **2-photon microscope for up to 24 hours**
1166 (A) *Nkx2.5eGFP*; *RERT*$^{+/-}$; *Rosa26Rtdtomato*$^{+/-}$ embryo. Starting culture at E7.5, by
1167 the end of the 25 hours ex-vivo culture, the HT has formed and looped (experiment
1168 repeated 3 times independently). The embryo was subsequently fixed and
1169 immunostained for cTnnT (red) and ZO-1 (blue). V: prospective left ventricle, A:
1170 prospective atria. Scale bars: 100µm.
1171
1172 **Figure 4-figure supplement 2. Quantification of the displacement of the**
1173 **splanchnic mesoderm during HT formation.**
1174 (A) z-max projection of a *Mesp1*$^{cre/+}$*; Rosa26Rtdtomato*$^{+/-}$ embryo at transversal HT
1175 stage. The yellow line indicates the distance between the left and right splanchnic
1176 mesoderm. (B) One example of the changes in left/right distance measured over time.
1177
1178 Figure Source Data 4
1179 Source data for Figure Figure 4-figure supplement 2
1180
1181
1182 **Figure 5. Live-imaging of cardiac differentiation at cellular resolution**
1183 (A) Time course of an *Nkx2.5eGFP*; *RERT*$^{cre/+}$; *Rosa26Rtdtomato*$^{+/-}$ embryo during
1184 stages when cc differentiation takes place -from EHF onwards-. Images are z-
1185 maximum projection of 76 sections acquired every 3µm covering 228µm. A bright-

1186 field image of the EHF embryo at the initial time point is also shown. (i, ii and iii)
1187 Rationale of the expected evolution of GFP expression: since tracks carry information
1188 on reporter expression, if a cell acquires a high level of GFP, we predict that it is
1189 committed to differentiate. See also Video 12. (B-D) Examples of time-lapse videos
1190 (B and C) and quantification of the GFP level (D) increasing in a single cell during
1191 differentiation (B) or remaining low in a cell located in the splanchnic mesoderm (C).
1192 A neural tube cell was additionally quantified (blue). Images are single optical
1193 sections. (E) Time course of individual cells tracked in the video shown in A. Cells
1194 with GFP levels above the median intensity value of all cells at the end of the
1195 recording are represented as green spheres and cells with lower GFP levels are shown
1196 as red spheres. (F) GFP level through time. Blue dotted line: median value (5249 a.u.).
1197 GFP level for each tracked cell was measured at five successive time points. Cell
1198 divisions are not represented for simplicity. (G) Normalized GFP level showing the
1199 relative increase in GFP levels for the GFP-positive cells at the end of the recording.
1200 Average increase: 2,77 fold ± 1.50, mean ± SD, n=95 cells from 3 independent videos.
1201 (H) The position of cells that differentiate (green) and cells that do not is shown in
1202 the cc at the initial time point (EHF stage). (I) The lineage from cardiac precursors
1203 share differentiation fate. Lineages of dividing progenitors (n=55 from 3 independent
1204 videos) were identified during early stages of cardiac differentiation. Two daughter
1205 cells are defined as sharing the same fate if their GFP intensity levels do not differ by
1206 more than 1.5 fold and/or both show levels above or below the threshold value
1207 defined. Scale bars: 100µm.
1208
1209 **Figure 5-figure supplement 1. Live-imaging of *Nkx2.5eGFP* reporter line**
1210 (A-C) Time-lapse video sequences of *Nkx2.5eGFP* embryos from Early Bud (A), cc
1211 (B) and open HT stage (C). Images are z-maximum projections of 75 sections
1212 acquired every 4µm covering 300µm in (A), 55 sections acquired every 6µm covering
1213 300µm in (B) and 59 sections acquired every 5µm covering 295µm in (C). (B' and
1214 C'): z-max projection covering 132µm (B') and 60µm (C') showing the dorsal
1215 opening and the dorsal closure of the HT at the end of the videos (representative of 3
1216 embryos). See also Videos 9 and 11. Scale bars: 100µm.
1217
1218 **Figure 5- figure supplement 2. Cells divide during cardiac differentiation**

1219 (A-C) Time-lapse video of a dividing tdtomato+ cell. Images are single optical
1220 sections (same embryo as shown in Figure 4A). The dividing tdtomato+ cell and
1221 daughter cells are segmented and mean GFP level is measured. (D) Full 4D track of
1222 the dividing cell showing close localization of the progeny in the cardiac crescent.
1223 Scale bars: 100µm.
1224
1225 **Figure 5- figure supplement 3.** Endocardial cells show an elongated shape. (A)
1226 Single optical section of a tamoxifen-induced *Nkx2.5eGFP*; *RERT*$^{+/-}$;
1227 *Rosa26Rtdtomato*$^{+/-}$ embryo showing a single endocardial labeled cell (white arrow).
1228 Scale bars: 100µm.
1229
1230 Figure Source Data 5
1231 Source data for Figure 5A, D, F, G, I and Figure 5-figure supplement 1C, D
1232
1233 **Figure 6. No cardiac differentiation is detected during early HT morphogenesis**
1234 (A-B) Initial and final time points of two time-lapse videos of tamoxifen-induced
1235 *Nkx2.5eGFP*; *RERT*$^{+/-}$; *Rosa26Rtdtomato*$^{+/-}$ embryos covering the transformation of
1236 the transversal HT into the open HT. Images are z-maximum projections of 44
1237 sections acquired every 5µm covering 220µm in (A) and of 46 sections acquired
1238 every 6µm covering 276µm in (B). See also Video 13. (C, D) GFP levels over time of
1239 the cells tracked in (A, B). GFP level for each tracked cell was measured at four
1240 successive time points. Green tracks represent cardiomyocytes with GFP intensity
1241 above the median intensity value of all the tracked cells at the last time point, while
1242 red tracks represent cells with lower GFP level. Blue dotted line represents the
1243 median intensity value (10748 a.u. in (C) and 12248a.u. in (D)). Note that when cells
1244 divide, only one of the two daughter cells was represented for simplicity. (E)
1245 Distribution of the tracked cells from the time-lapse video shown in (A) at the initial
1246 and final times of the tracking period. tdtomato+, GFP- cells are represented by red
1247 spheres and tdtomato+, GFP+ cells are represented by green spheres. (F) Example of
1248 tdtomato+ cardiomyocytes tracked in the beating ventricle. (G) Normalized
1249 progression of GFP level in cells classified as GFP+ showing stable GFP levels. Data
1250 collected from 125 tracked cells from four independent videos of 2h52m to 3h12m
1251 duration. Average increase: 1,1 fold ± 0.28, mean ± SD. (H) Magnification extracted

1252 from the video in A (yellow inset) of tdtomato+ cells in the boundary zone between
1253 the undifferentiated and differentiated cells. (I) Quantification of GFP level through
1254 time of the three segmented cells shown in (H). Cells show stable GFP levels and do
1255 not differentiate. Images are z-maximum projections of 6 sections acquired every
1256 5µm covering 30µm. Scale bars: 100µm.
1257
1258 **Figure 6- figure supplement 1.**
1259 Longer videos can capture both initial cardiac differentiation in the FHF and early HT
1260 morphogenesis. (A) Initial and final images from a time-lapse video of a tamoxifen-
1261 induced *RERT*$^{+/-}$*; Rosa26Rtdtomato*$^{+/-}$*; Nkx2.5eGFP* embryo. Images are z-maximum
1262 projection of 44 sections acquired every 5µm covering 220µm. (B) GFP levels over
1263 time of the cells tracked in (A). GFP level for each tracked cell was measured at five
1264 successive time points. Green tracks represent cells with GFP intensity above the
1265 median intensity value of all the tracked cells at the last time point, while red tracks
1266 represent cells that maintain lower GFP levels. The blue dotted line represents the
1267 median intensity value. (C) Mean intensity value for all the green and red tracks and
1268 SD. Note that on average the GFP intensity of the green tracks becomes stable from
1269 around the transversal HT stage (around t=300m). Scale bars: 100µm.
1270
1271 Figure Source Data 6
1272 Source data for Figure 6A, B, C, D, G, I, Figure 6-figure supplement 1A, Figure 6-
1273 figure supplement 1B and C.
1274
1275 **Figure 7. No cardiac differentiation is detected during early HT morphogenesis.**
1276 (A-A'') Time-lapse video of a tamoxifen-induced *RERT*$^{+/-}$*; Rosa26Rtdtomato*$^{+/-}$*;*
1277 *Nkx2.5eGFP* embryo during the stages at which the transversal HT transforms into an
1278 open HT, showing cells located in the splanchnic mesoderm (white arrows in A' and
1279 A''), respecting the boundary with the HT (yellow arrows in J' show two cells located
1280 in the HT). Lower doses of tamoxifen were injected in order to label only a very small
1281 proportion of cells in red. Images are z-maximum projection of 74 sections (A)
1282 acquired every 4µm covering 296µm and (A') 7 sections covering 28µm. (A'') 3D
1283 reconstruction based of the *Nkx2.5eGFP* signal (green) and tdtomato+ cells located in
1284 the splanchnic mesoderm. See also Video 14. Scale bars: 100µm. Splan. meso:

1285 splanchnic mesoderm.

1286

1287 **Figure 8. SHF Isl1-expressing cells do not contribute to the early open-heart tube.**
1288 (A) Time-lapse video sequences of an *Isl1$^{cre/+}$; Rosa26Rtdtomato$^{+/-}$; Nkx2.5eGFP*
1289 embryo showing that recombination driven by *Islet1^{cre}* of the *Rosa26* locus is
1290 complete in the splanchnic mesoderm and scarce in the FHF (n=3 videos from cc up
1291 to open HT stage). (B) Inset from A (yellow frame). Two cells of the Isl1+ lineage
1292 located in the cc increase their tdtomato level over time. (C) Inset from A (Red
1293 frame); increase of the tdtomato intensity in the splanchnic mesoderm over time.
1294 Arrow shows the boundary between SHF and FHF and points to a single cell in the
1295 SHF that retains a low level of GFP and a columnar shape. Note that tdtomato signal
1296 is also detectable in the endoderm. Images are z-maximum projection of 45 sections
1297 acquired every 5µm and covering 225µm in (A) and of 6 sections covering 30µm in
1298 (C). See also Videos 15-16. (D) Same embryo as in (A) post-fixed and
1299 immunostained against cTnnT after live-imaging, showing that the red cells located in
1300 the splanchnic mesoderm are undifferentiated. Scale bars: 100µm.

1301

1302 **Figure 8- figure supplement 1. GFP level in deeper z levels cannot be accurately**
1303 **quantified.**
1304 (A-A'') *RERT$^{+/-}$; Rosa26Rtdtomato$^{+/-}$; Nkx2.5eGFP* embryo at transversal HT stage.
1305 (A) z-maximum projection of 74 sections acquired every 4µm and covering 296µm.
1306 Same embryo as in Figure 6A. (A') Single optical z-section positioned at the white
1307 dotted line shown in (A). This z-section shows the green signal decay at deep z
1308 positions (z= 0 to -274µm). (A'') An xy frame corresponding to a -272μm z-position
1309 (indicated by the red dotted line in (A') at different time points during the video. The
1310 white arrow indicates td-tomato+ cells.

1311

1312 **Figure 8- figure supplement 2. Cells increasing their GPF expression can be**
1313 **detected at the venous pole during activation of SHF contribution to the HT.**
1314 (A) Time course of a tamoxifen-induced *RERT$^{+/-}$; Rosa26Rtdtomato$^{+/-}$; Nkx2.5eGFP*
1315 embryo during linear HT formation. Images are z-maximum projection of 44 sections
1316 acquired every 5µm covering 220µm. (B) Time course of individual cells tracked
1317 within the yellow-framed region in video (A). (C) GFP levels over time of the cells

1318 tracked in (B) Cell 1 shows high GFP level throughout the video while cell 2 and 3
1319 increase their GFP level over time. The blue line represents a neural tube cell. The
1320 dotted line marks the 1h30m time point. Scale bars100µm.
1321
1322 Figure Source Data 8
1323 Source data for Figure 8-figure supplement 2C.
1324
1325
1326 **Figure 9. SHF Isl1-expressing cells contribute to the arterial pole during late**
1327 **linear HT morphogenesis.**
1328 (A, B) *Isl1$^{cre/+}$; Rosa26Rtdtomato$^{+/-}$; Nkx2.5eGFP* embryos showing no contribution
1329 of the Isl1 lineage to the transversal HT (A-A'') but contributing robustly to the
1330 arterial pole and dorsal aspect of the linear HT (B- B''). The presence of double-
1331 positive cells in these areas reveals the differentiation of Isl1 lineage cells into
1332 cardiomyocytes (A, B). Images are 74 and 134 optical sections acquired every 2.5µm
1333 and covering 195µm and 335µm, respectively. In (B, B') only the double-positive
1334 cells located in the linear HT are shown, while the tdtomato+ progenitors, located
1335 outside the linear HT are not shown. Lateral views are shown in (A', B') including 3D
1336 reconstructions. (A'') Cross-sections in xy along the dotted lines shown in (A').
1337 Dorsal views are shown in (B'') including the 3D reconstruction of the tdtomato+
1338 cells located in the linear HT. White arrows show the dorsal (mesocardial) regions of
1339 the linear HT. (C) Snapshots of an *Ils1$^{cre/+}$; Rosa26Rtdtomato$^{+/-}$; Nkx2.5eGFP* embryo
1340 at different time points during the third phase showing that the tdtomato+ SHF cells
1341 contribute to the arterial pole of the HT. Images are 52 optical sections acquired every
1342 5µm and covering 260µm. The embryo was imaged continuously every 13m for the
1343 first 6h of culture and then imaged once again at time point 9h30m. Note that at the
1344 last time point, the laser was increased at maximum power in order to reveal more
1345 clearly the red labeled cells at the arterial pole. The contrast had to be enhanced as
1346 well. (C') Images at time points 0, 4h48m and 9h30m. Images at time points 0 and
1347 4h48m are z-maximum projection of 5 sections covering 25 µm. Image at 9h30m is a
1348 single optical section. at: arterial pole. endo: endoderm, splan meso: splanchnic
1349 mesoderm. Scale bars: 100µm.
1350

1351 **Figure 10. A model of cardiomyocyte differentiation dynamics during early heart**
1352 **development**
1353 We propose that two distinct phases of cardiomyocyte differentiation take place
1354 during early heart development. At EHF stage the cc differentiates and starts folding.
1355 Cardiomyocytes round up and become contractile while the cardiac progenitors
1356 located in the splanchnic mesoderm remain undifferentiated. Subsequently, the cc.
1357 undergoes further morphogenesis to transform into a HT, initially open dorsally and
1358 no cardiomyocyte differentiation is detected during this transformation. Finally,
1359 cardiac differentiation resumes contributing new cardiomyocytes from the splanchnic
1360 mesoderm to the arterial pole (prospective RV) and the dorsal closure of the HT.
1361
1362 **VIDEO LEGENDS:**
1363
1364 Video 1: 3D reconstruction of the cardiac crescent at EHF stage, based on *Nkx2.5*$^{cre/+}$
1365 *Rosa26Rtdtomato*$^{+/-}$ signal. Related to Figure 1A.
1366
1367 Video 2: 3D reconstruction of Mouse HT formation, based on embryos
1368 immunostained for cTnnT. Five representative stages are represented. Related to
1369 Figure 1C-G.
1370
1371 Video 3: 3D reconstruction of the FHF (green) and SHF (red). Based on *Nkx2.5*$^{cre/+}$
1372 *Rosa26Rtdtomato*$^{+/-}$ embryos immunostained for cTnnT. The border between cTnnT-
1373 negative and cTnnT-positive cells can be visualized at the interface between the red
1374 and green domains. Related to Figure 2B.
1375
1376 Video 4: z-maximum projection of an *Nkx2.5*$^{cre/+}$ *;Rosa26RmT/mG*$^{+/-}$ embryo at cc
1377 stage and single-section time-lapse video of the same embryo after 10h 42m of ex-
1378 vivo culture (representative analysis from 3 embryos). Interval between frames: 1s.
1379 Related to Figure 4E.
1380
1381 Video 5: Time-lapse video of a *Mesp1*$^{cre/+}$*; Rosa26Rtdtomato*$^{+/-}$ embryo from cc up to
1382 open HT stage (h:mm:ss) (representative analysis from 4 embryos). Interval between
1383 frames: 4m 30. Duration of the video: 13h 16m 30s. Related to Figure 4F.

1384

1385 Video 6: Same embryo as in Video 5. Images are z-maximum projection of 9 sections
1386 acquired every 4µm covering 36µm (h:mm:ss) and allows visualization of the inside
1387 of the cardiac lumen during HT formation. Interval between frames: 4m 30s. Duration
1388 of the video: 8h 10m. Related to Figure 4F'.

1389

1390 Video 7: Time-lapse video of an *Nkx2.5*$^{cre/+}$*; Rosa26RmT/mG*$^{+/-}$ embryo (h:mm:ss)
1391 (representative analysis from 2 embryos). Interval between frames: 22m. Duration of
1392 the video: 4h 02m. Related to Figure 4G-G'.

1393

1394 Video 8: Brightfield time-lapse video of a wild type embryo, from cc stage showing
1395 the onset of cardiomyocyte contractility and the formation of the cardiac lumen
1396 (h:mm:ss) (representative analysis from 2 embryos). Interval between frames: 1m 03s.
1397 Duration of the video: 6h 04m 21s. Representative analysis from 2 embryos.

1398

1399 Video 9: Same embryo shown in Video 14 zoomed-in at the level of the splanchnic
1400 mesoderm (mm:ss). SHF cells (green arrows) displace antero-medially relative to the
1401 underlying endoderm (red arrow). In addition, SHF cells move apart from each other
1402 (distance between the green arrows increase from 61 to 83µm over 3h12m). Related
1403 to Figure 6H and Figure 6- figure supplement 6A.

1404

1405 Video 10: Time-lapse video sequences of *Nkx2.5eGFP* embryos from Early Bud/E7.5
1406 stage (h:mm:ss). (representative analysis from 2 embryos). Interval between frames:
1407 12m. Duration of the video: 7h 24m Related to Figure 5-figure supplement 1A.

1408

1409 Video 11: Time-lapse video sequences of *Nkx2.5eGFP* embryos from cc to
1410 transversal HT stage (h:mm:ss). (representative analysis from 3 embryos). Interval
1411 between frames: 24m. Duration of the video: 6h 48m. Related to Figure 4H.

1412

1413 Video 12: Time-lapse video sequences of *Nkx2.5eGFP* embryos from transversal HT
1414 to open HT stage (h:mm:ss) (representative analysis from 3 embryos). Interval
1415 between frames: 8m 09s. Duration of the video: 5h 01m 33s. Related to Figure5 -
1416 figure supplement 1B.

1417

1418 Video 13: Cell tracks in 3D+t during stages when cc differentiation takes place -from
1419 EHF onwards- (h:mm:ss). Cells are represented as green spheres if considered GFP+
1420 at the end of the time-lapse analysis. and as red spheres when considered GFP-
1421 (Representative analysis from 3 embryos). Interval between frames: 19m 18s
1422 Duration of the video: 5h 28m 06s. Related to Figure 5A.

1423

1424 Video 14: Cell tracks in 3D+t during stages the open HT forms. Cells are represented
1425 as green spheres if considered GFP+ at the end of the time-lapse analysis and as red
1426 spheres when considered GFP-(Representative analysis from 3 embryos). Interval
1427 between frames: 7m 40s. Duration of the video: 3h 12m. Related to Figure 6A.

1428

1429 Video 15: Time-lapse video of a *RERT*$^{+/-}$*; Rosa26Rtdtomato*$^{+/-}$*; Nkx2.5eGFP* embryo
1430 during the stages at which the transversal HT transforms into the open HT (h:mm:ss).
1431 Interval between frames: 19m 19s. Duration of the video: 7h 24m 35s. (2nd half) 3D
1432 reconstruction at three time points based of the eGFP signal (green) and red-labeled
1433 cells located in the splanchnic mesoderm. Related to Figure 7A.

1434

1435 Video 16: Time-lapse video of an *Isl1*$^{cre/+}$*; Rosa26Rtdtomato*$^{+/-}$*; Nkx2.5eGFP* embryo
1436 (h:mm:ss) (representative analysis from 3 embryos). Interval between frames: 6m.
1437 Duration of the video: 7h 18m. Related to Figure 8A.

1438

1439 Video 17: Same embryo shown in Video 16 zoomed-in at the level of the splanchnic
1440 mesoderm (h:mm:ss). Related to Figure 8C.

1441

1442 Video 18: 3D rendering of an *Isl1*$^{cre/+}$*;Rosa26Rtdtomato*$^{+/-}$*; Nkx2.5eGFP* embryo at
1443 transversal HT stage. Related to Figure 9A.

1444

1445 Video 19: 3D rendering of an *Isl1*$^{cre/+}$*;Rosa26Rtdtomato*$^{+/-}$*; Nkx2.5eGFP* embryo at
1446 linear HT stage. Related to Figure 9B.

Figure 1

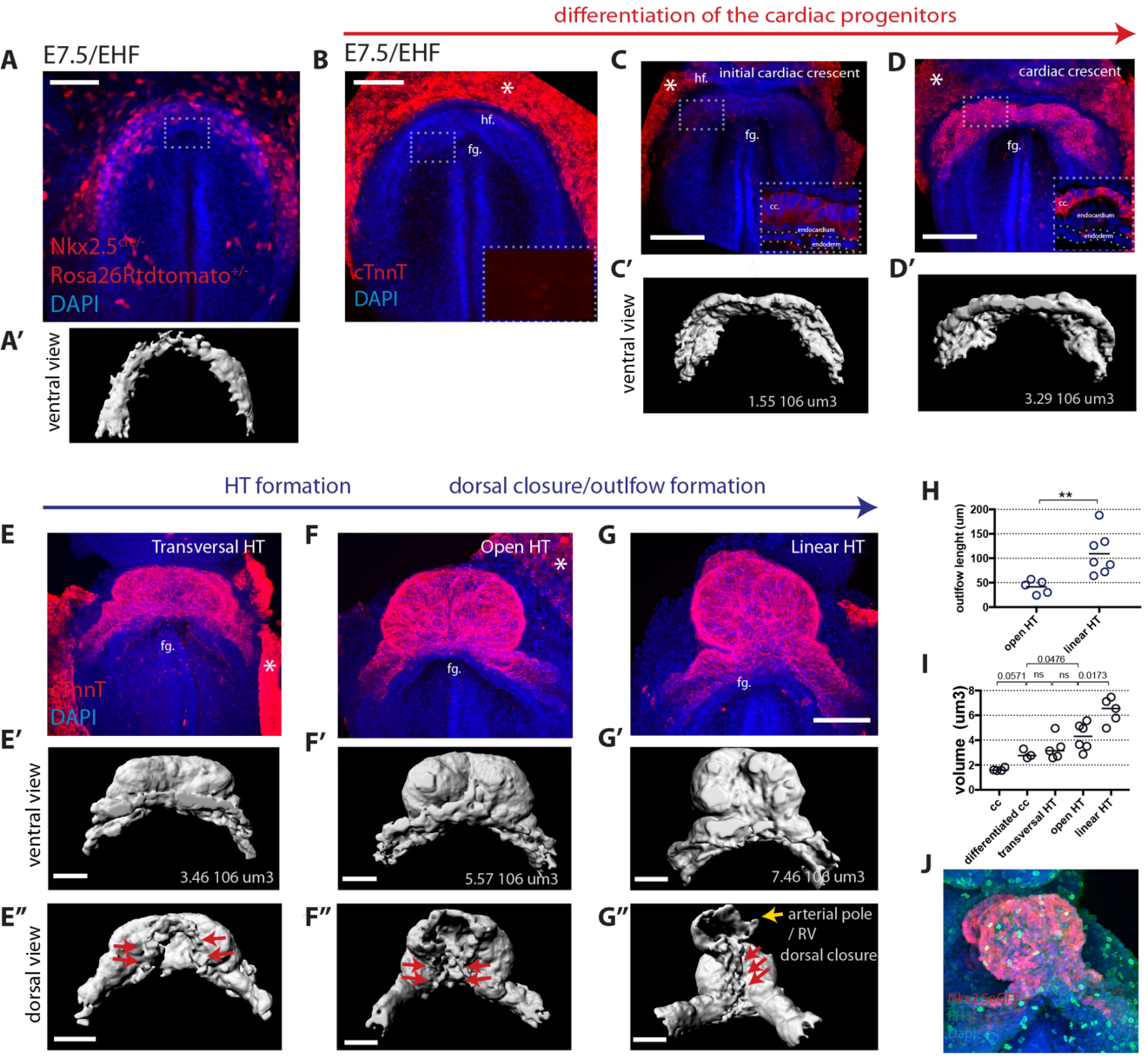
differentiation of the cardiac progenitors
A
E7.5/EHF
Nkx2.5cre+/-
Rosa26Rtdtomato+/-
DAPI
A'
ventral view
B
E7.5/EHF
hf.
fg.
cTnnT
DAPI
C
initial cardiac crescent
hf.
fg.
cc.
endocardium
endoderm
C'
ventral view
1.55 106 um3
D
cardiac crescent
fg.
cc.
endocardium
endoderm
D'
3.29 106 um3
HT formation
dorsal closure/outlfow formation
E
Transversal HT
fg.
cTnnT
DAPI
E'
ventral view
3.46 106 um3
E''
dorsal view
F
Open HT
fg.
F'
5.57 106 um3
F''
G
Linear HT
fg.
G'
7.46 106 um3
G''
arterial pole
/ RV
dorsal closure
H
outflow lenght (um)
200
150
100
50
0
**
open HT
linear HT
I
volume (um3)
8
6
4
2
0
0.0571
ns
ns
0.0476
0.0173
cc
differentiated cc
transversal HT
open HT
linear HT
J
Nkx2.5eGFP
Dapi

Figure 1- figure supplement 1

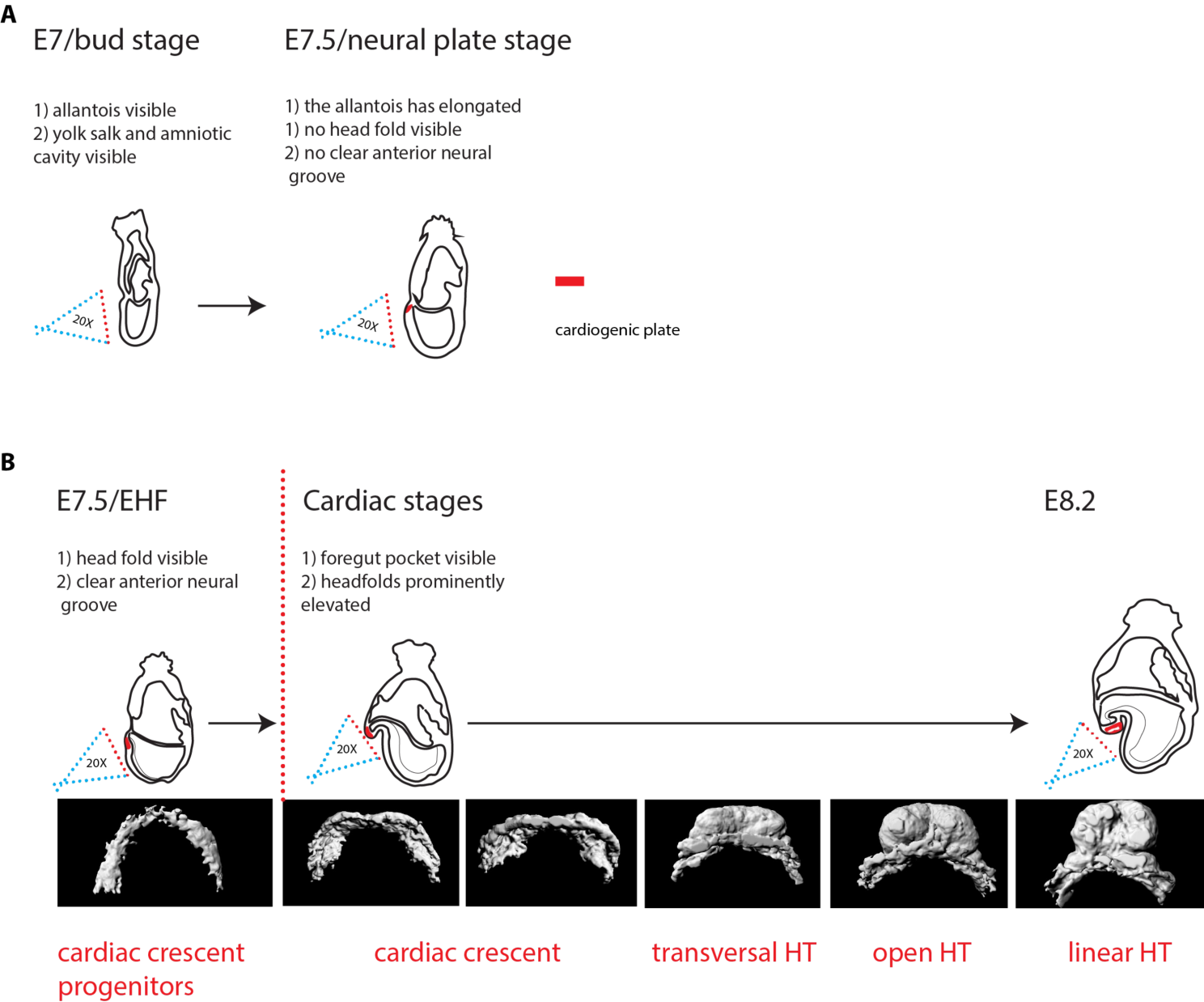

Figure 1- figure supplement 2

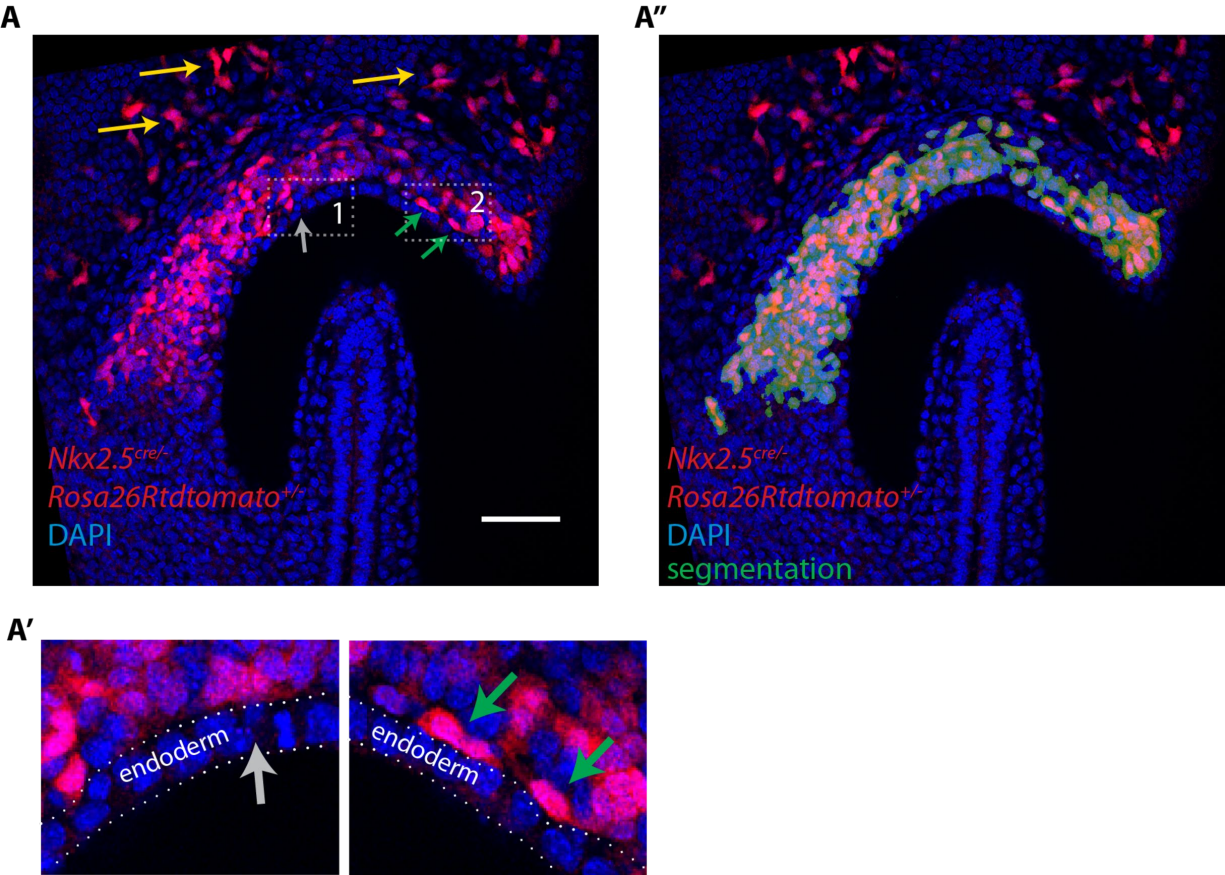

Figure 1- figure supplement 3

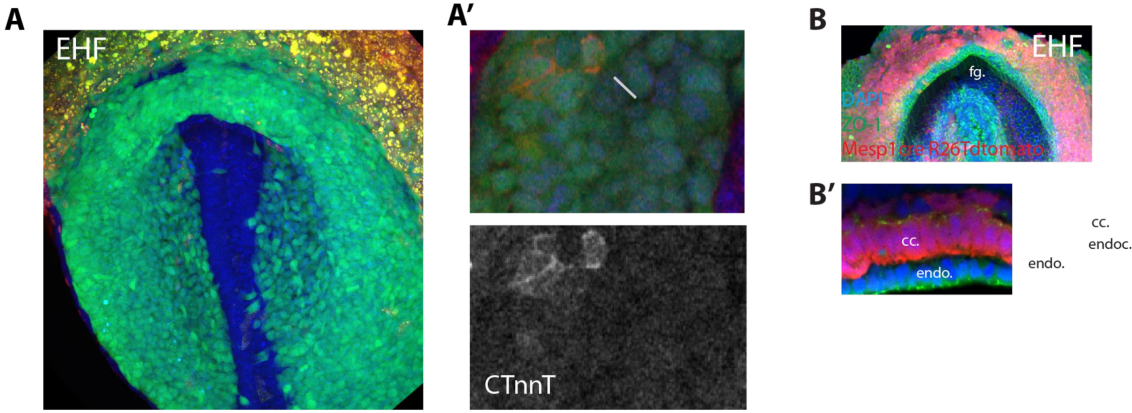

Mesp1$^{cre/-}$ *Rosa26Rtdtomato*$^{+/-}$
cTnnT
Dapi

Figure 2

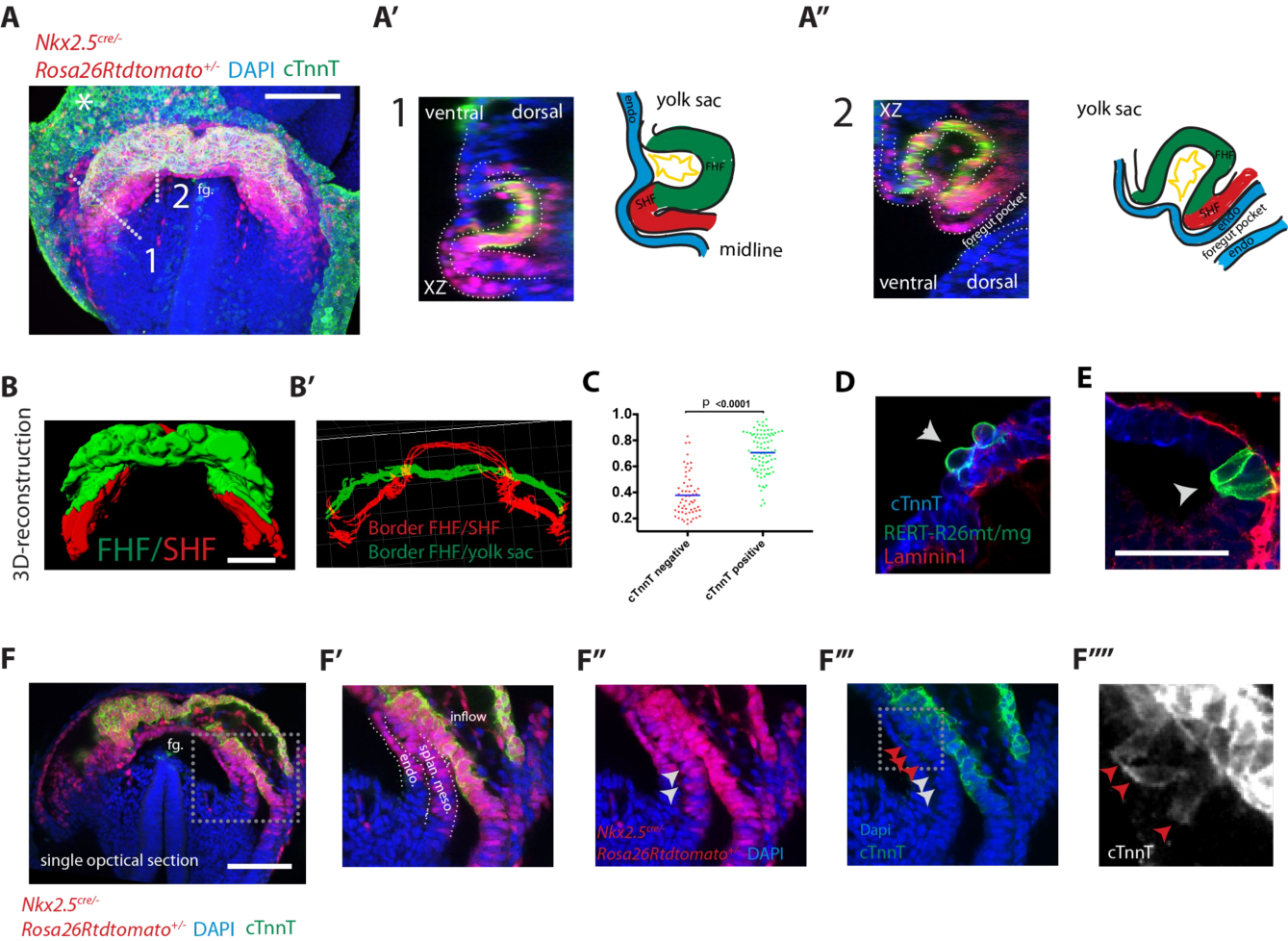
A
Nkx2.5cre/-
Rosa26Rtdtomato+/- DAPI cTnnT
*
2
fg.
1
A'
1
ventral
dorsal
XZ
yolk sac
endo
FHF
SHF
midline
A''
2
XZ
ventral
dorsal
foregut pocket
yolk sac
FHF
SHF
endo
foregut pocket
endo
B
3D-reconstruction
FHF/SHF
B'
Border FHF/SHF
Border FHF/yolk sac
C
p <0.0001
1.0
0.8
0.6
0.4
0.2
cTnnT negative
cTnnT positive
D
cTnnT
RERT-R26mt/mg
Laminin1
E
F
fg.
single opctical section
Nkx2.5cre/-
Rosa26Rtdtomato+/- DAPI cTnnT
F'
inflow
endo.
splan. meso.
F''
Nkx2.5cre/-
Rosa26Rtdtomato+/- DAPI
F'''
Dapi
cTnnT
F''''
cTnnT

Figure 2- figure supplement 1

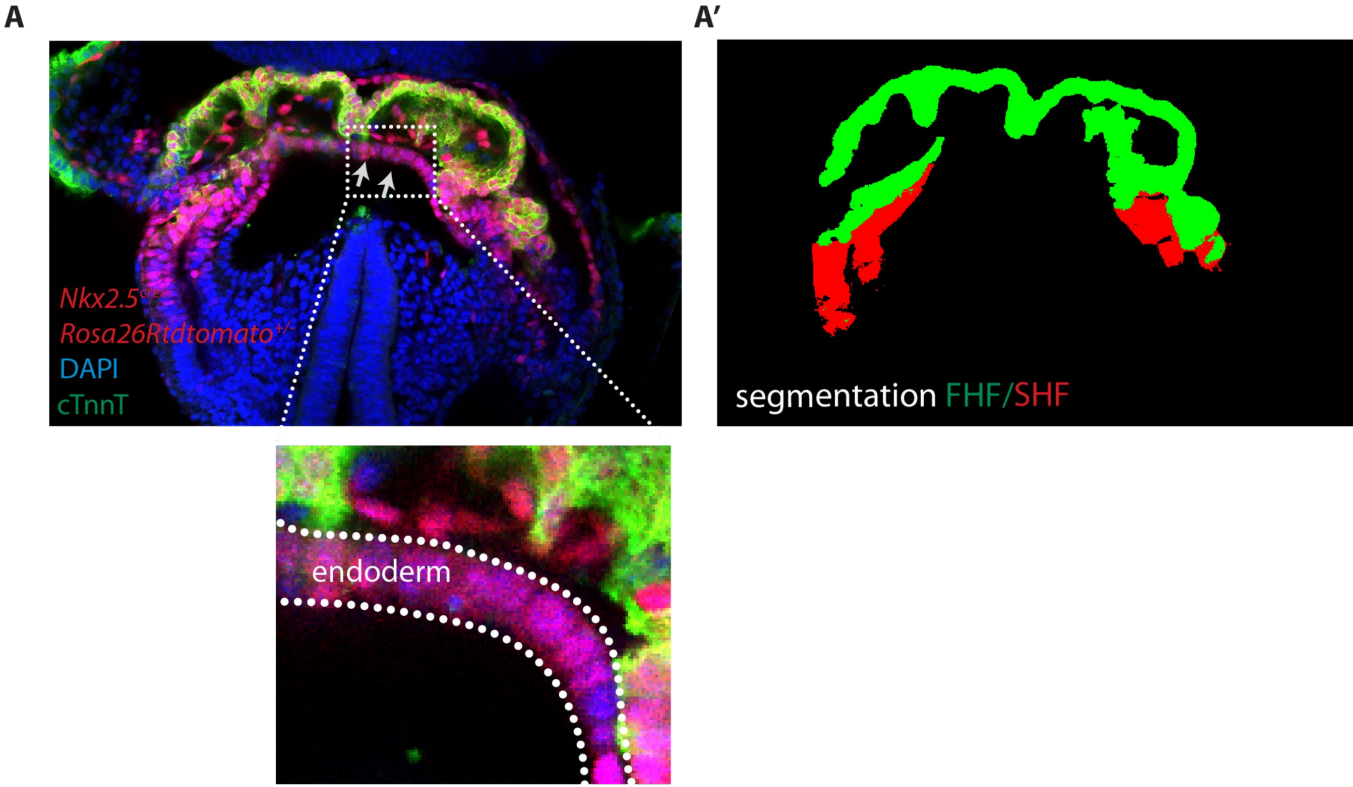

Figure 2- figure supplement 2

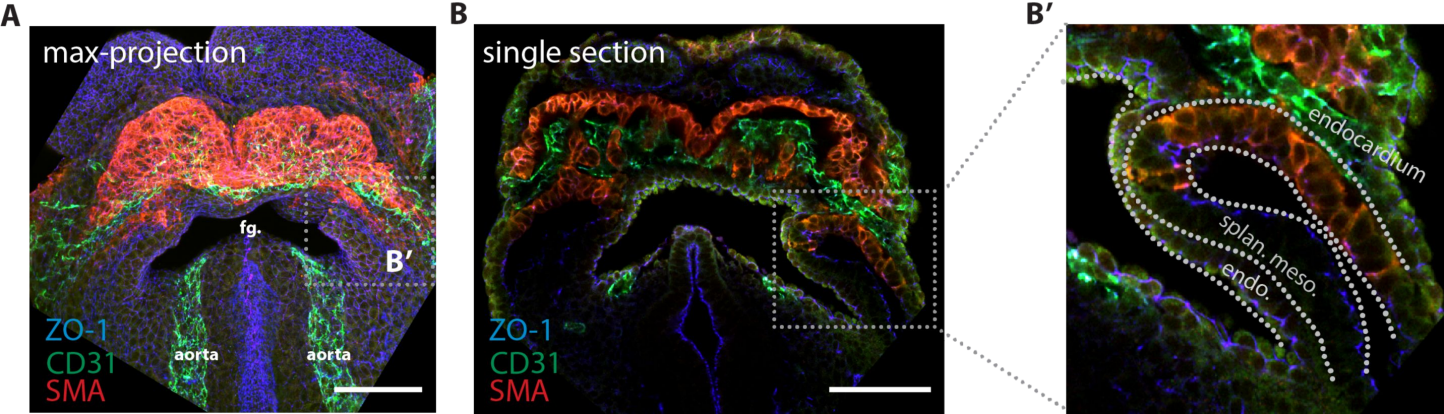

Figure 3

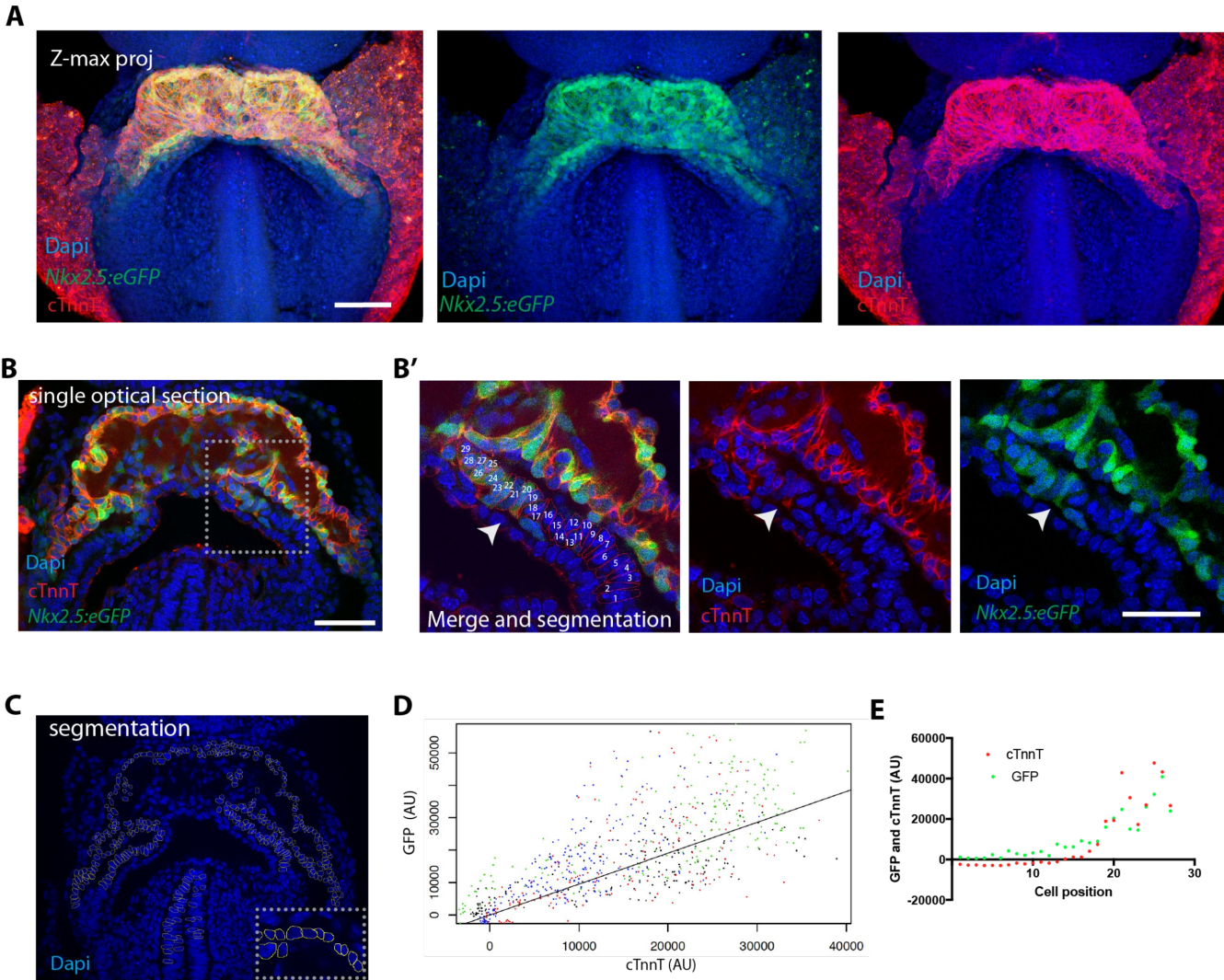
A
Z-max proj
Dapi
Nkx2.5:eGFP
cTnnT
Dapi
Nkx2.5:eGFP
Dapi
cTnnT
B
single optical section
Dapi
cTnnT
Nkx2.5:eGFP
B'
Merge and segmentation
Dapi
cTnnT
Dapi
Nkx2.5:eGFP
C
segmentation
Dapi
D
GFP (AU)
cTnnT (AU)
E
cTnnT
GFP
GFP and cTnnT (AU)
Cell position

Figure 3- figure supplement 1

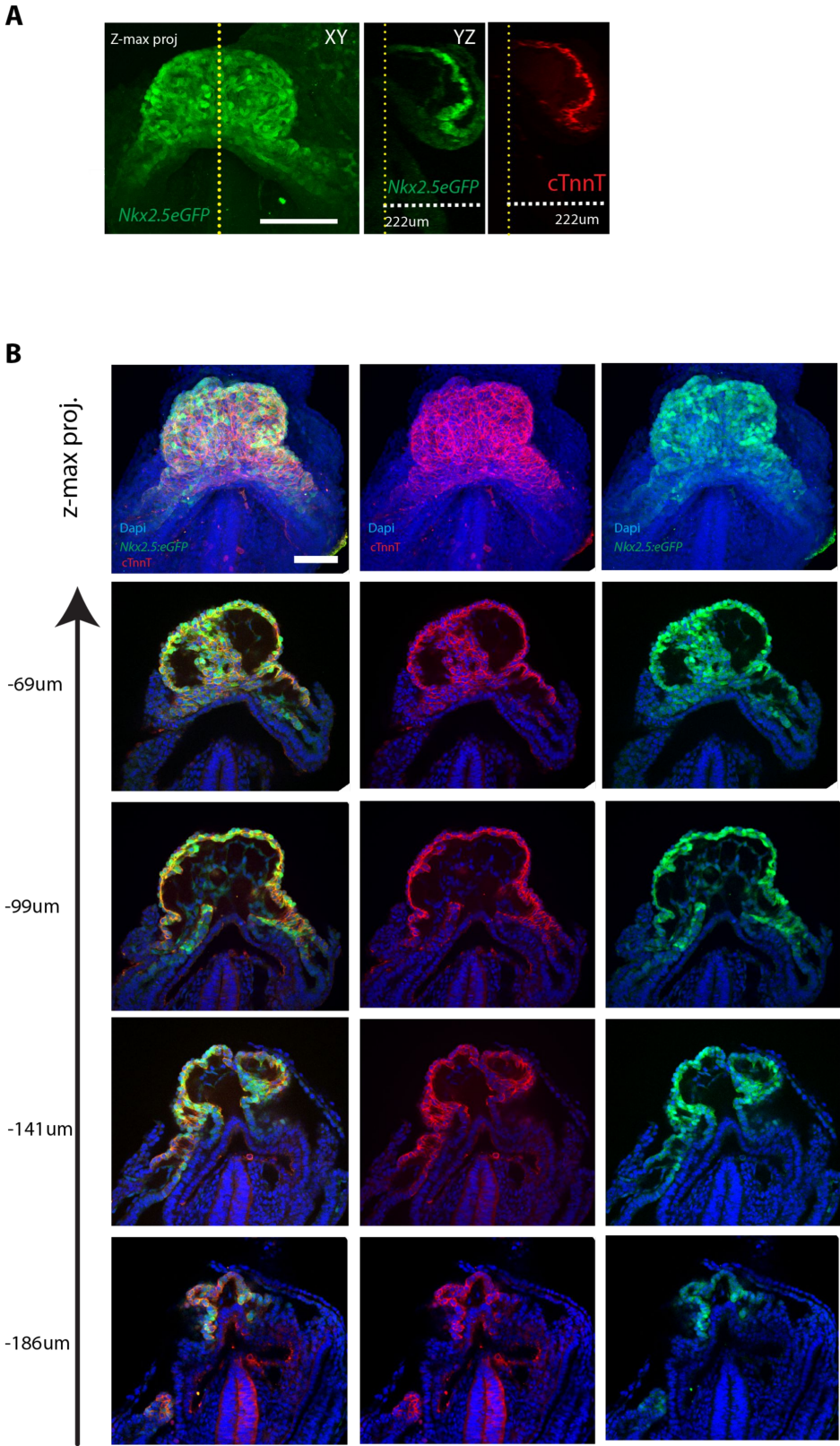

Figure 3- figure supplement 2

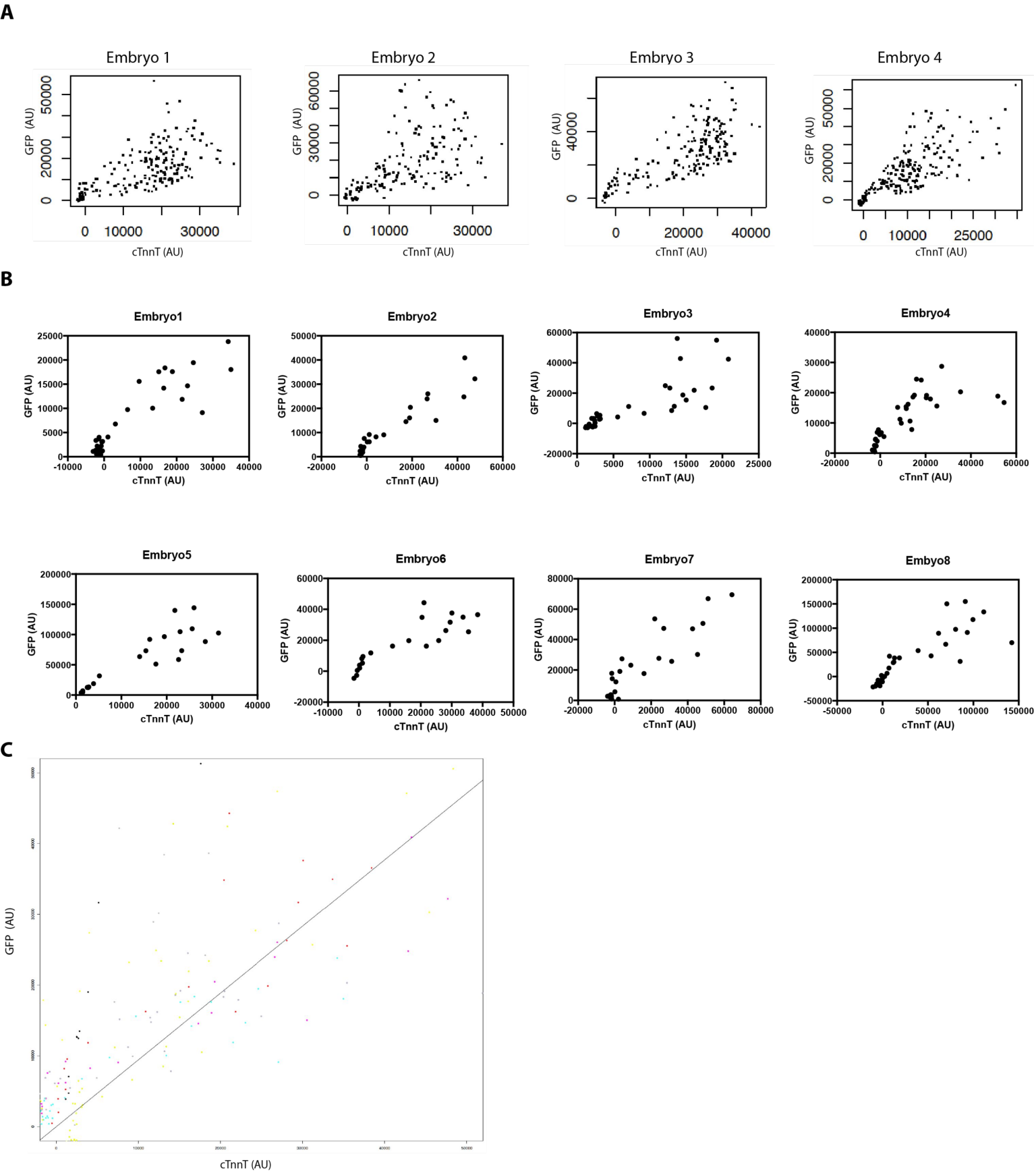

Figure 3- figure supplement 3

A

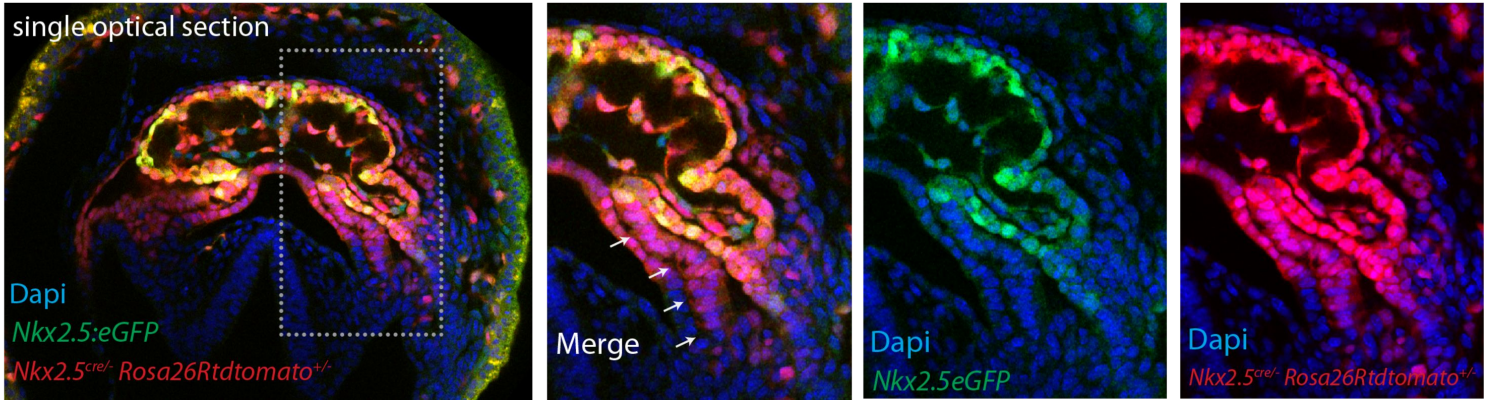

Figure 4

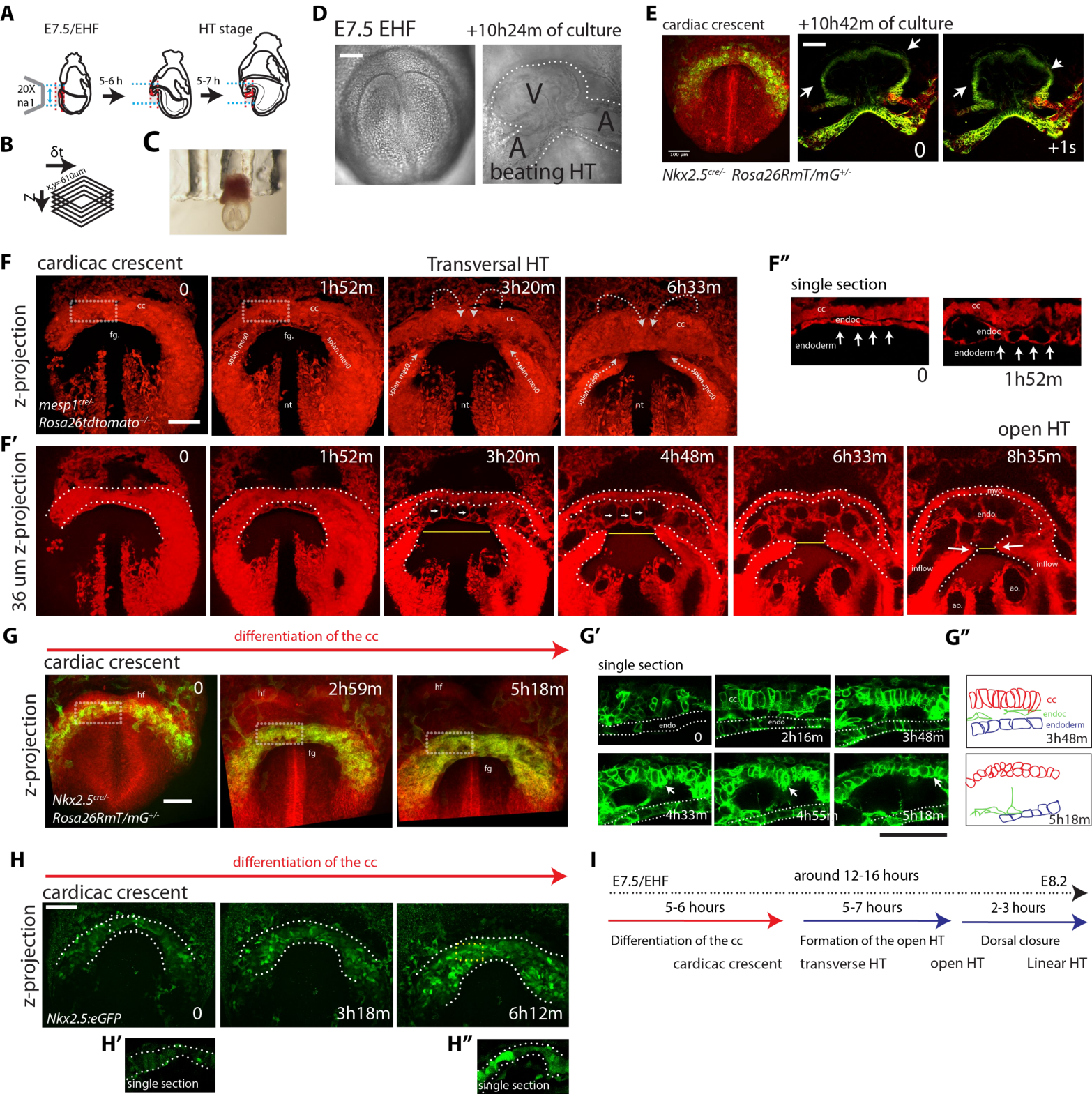
A
E7.5/EHF
HT stage
20X
na1
5-6 h
5-7 h
B
δt
x,y=610um
z
C
D
E7.5 EHF
+10h24m of culture
V
A
A
beating HT
E
cardiac crescent
+10h42m of culture
0
+1s
Nkx2.5cre/- Rosa26RmT/mG+/-
F
cardiac crescent
Transversal HT
z-projection
0
1h52m
3h20m
6h33m
cc
fg.
nt
splan. meso
mesp1cre/-
Rosa26tdtomato+/-
F''
single section
cc
endoc
endoderm
0
1h52m
F'
open HT
36 um z-projection
0
1h52m
3h20m
4h48m
6h33m
8h35m
myo.
endo.
inflow
ao.
G
differentiation of the cc
cardiac crescent
z-projection
0
2h59m
5h18m
hf
fg
Nkx2.5cre/-
Rosa26RmT/mG+/-
G'
single section
endo
cc
0
2h16m
3h48m
4h33m
4h55m
5h18m
G''
cc
endoc
endoderm
3h48m
5h18m
H
differentiation of the cc
cardiac crescent
z-projection
Nkx2.5:eGFP
0
3h18m
6h12m
H'
single section
H''
single section
I
E7.5/EHF
around 12-16 hours
E8.2
5-6 hours
5-7 hours
2-3 hours
Differentiation of the cc
Formation of the open HT
Dorsal closure
cardiac crescent
transverse HT
open HT
Linear HT

Figure 4- figure supplement 1

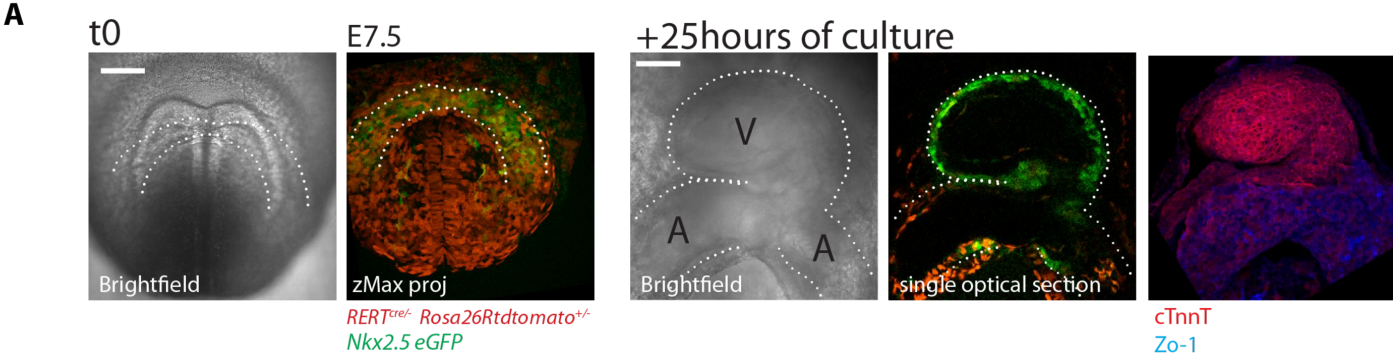

Figure 4- figure supplement 2

A

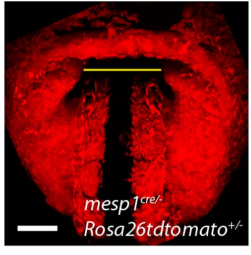

B

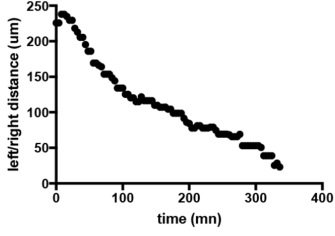

Figure 5

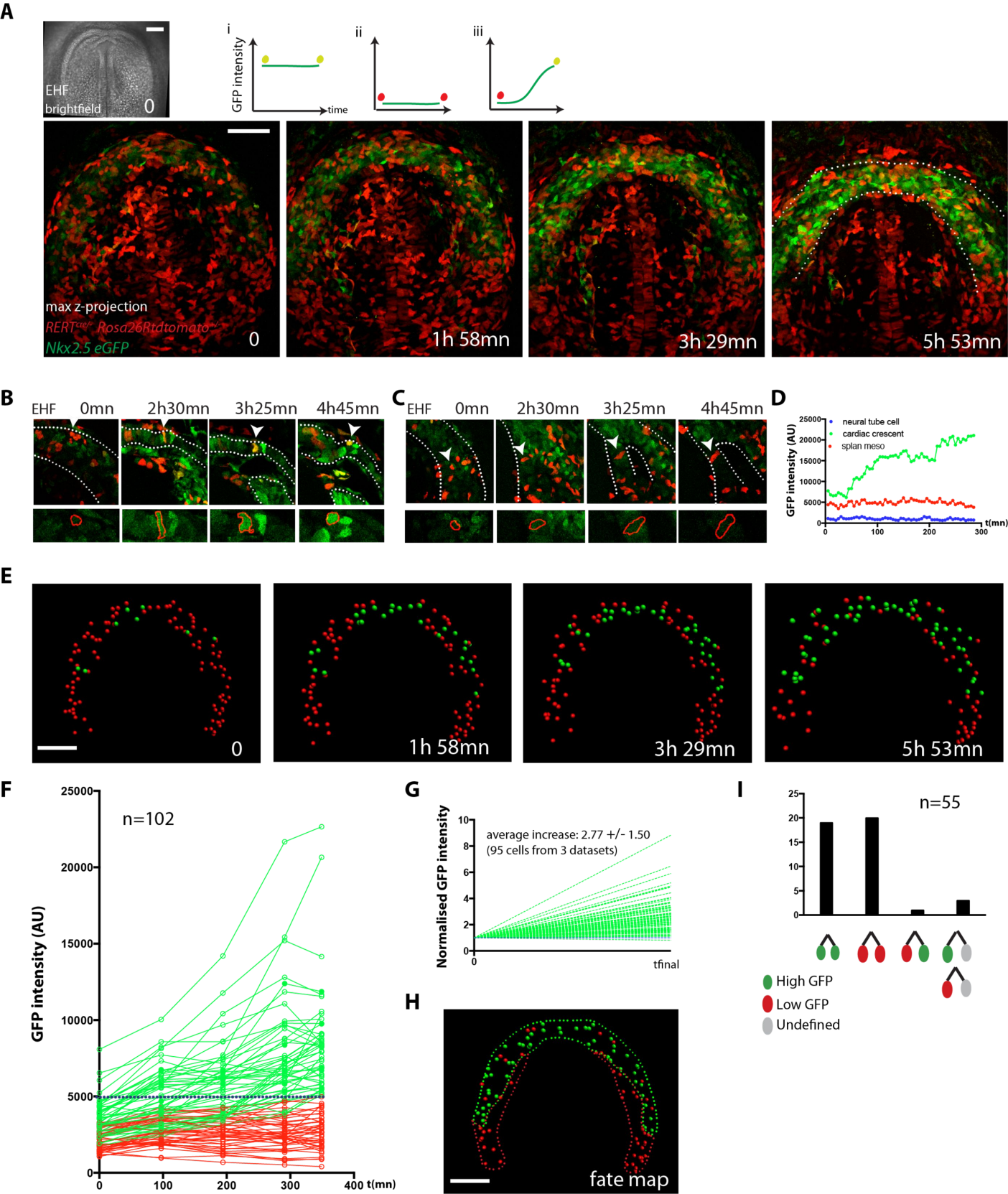
A
EHF
brightfield
0
i
ii
iii
GFP intensity
time
max z-projection
RERT^cre/+ Rosa26Rtdtomato+/-
Nkx2.5 eGFP
0
1h 58mn
3h 29mn
5h 53mn
B
EHF
0mn
2h30mn
3h25mn
4h45mn
C
EHF
0mn
2h30mn
3h25mn
4h45mn
D
neural tube cell
cardiac crescent
splan meso
GFP intensity (AU)
t(mn)
E
0
1h 58mn
3h 29mn
5h 53mn
F
n=102
GFP intensity (AU)
t(mn)
G
average increase: 2.77 +/- 1.50
(95 cells from 3 datasets)
Normalised GFP intensity
tfinal
H
fate map
I
n=55
High GFP
Low GFP
Undefined

Figure 5- figure supplement 1

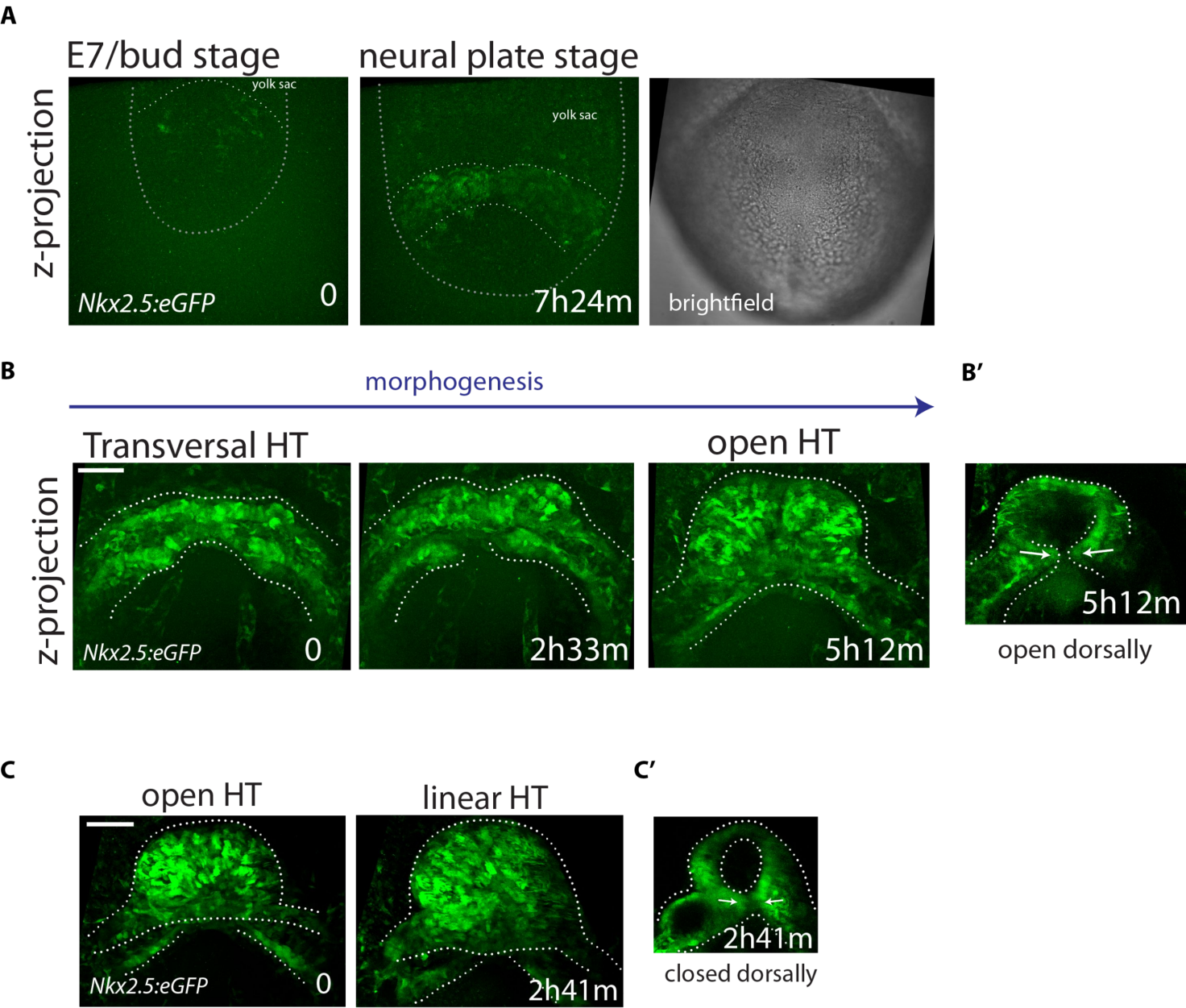

Figure 5- figure supplement 2

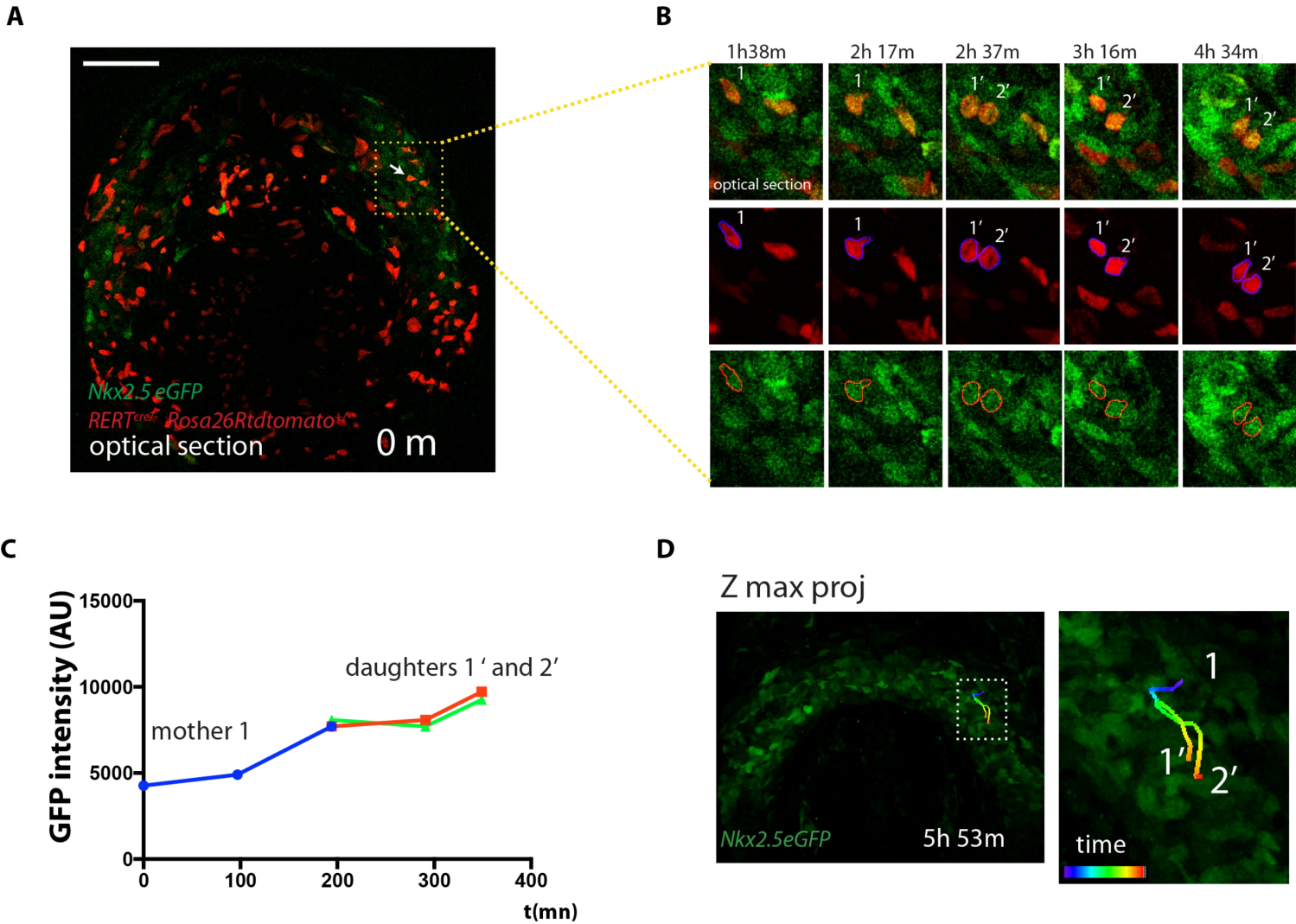

Figure 5- figure supplement 3

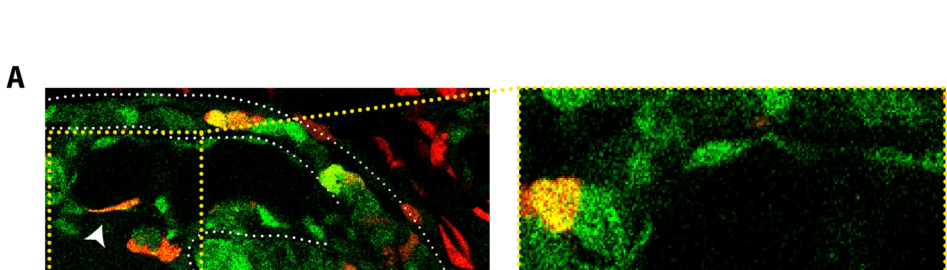

Figure 6

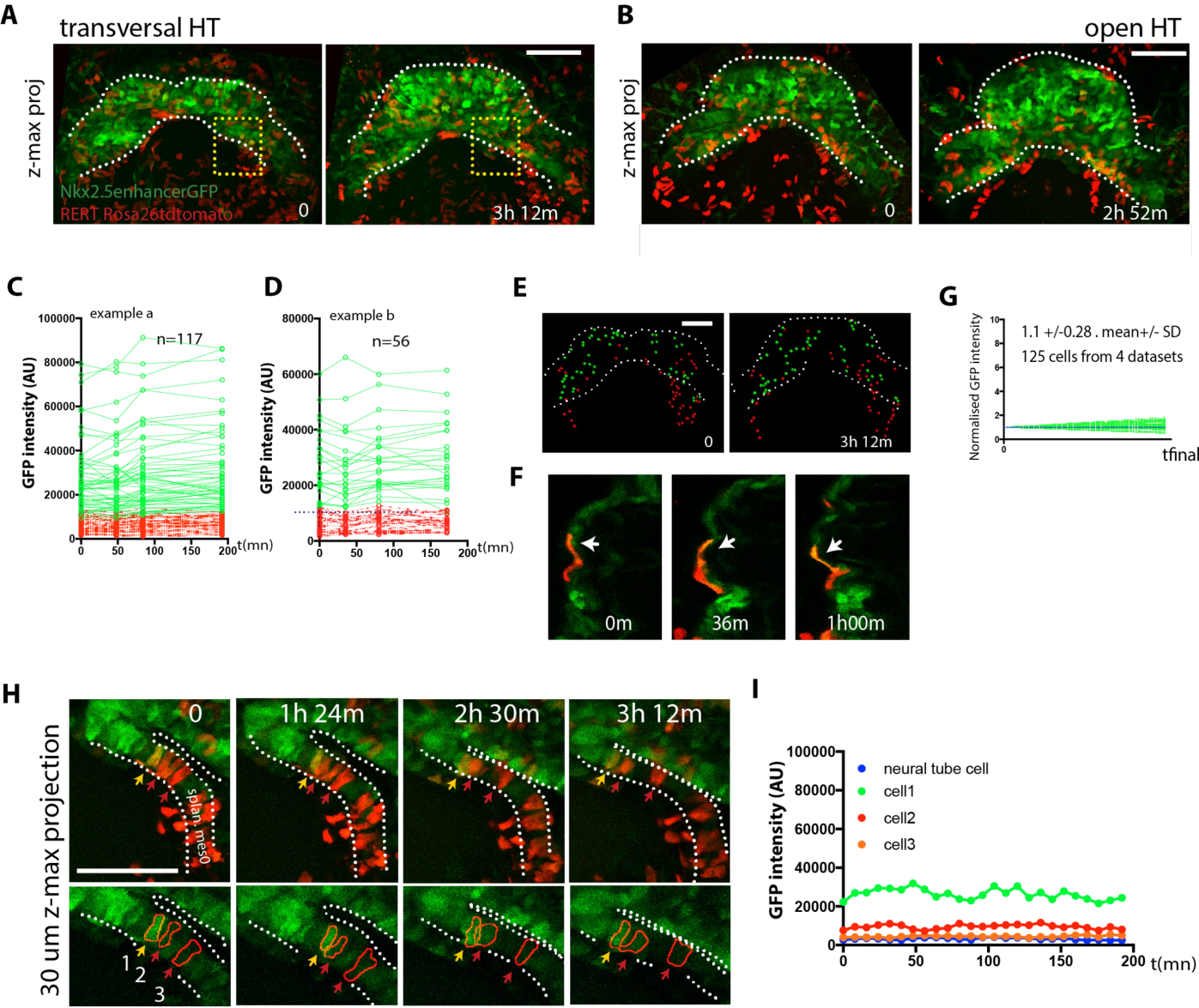
A
transversal HT
z-max proj
Nkx2.5enhancerGFP
RERT Rosa26tdtomato
0
3h 12m
B
open HT
z-max proj
0
2h 52m
C
example a
n=117
GFP intensity (AU)
t(mn)
D
example b
n=56
GFP intensity (AU)
t(mn)
E
0
3h 12m
F
0m
36m
1h00m
G
1.1 +/-0.28 . mean+/- SD
125 cells from 4 datasets
Normalised GFP intensity
tfinal
H
0
1h 24m
2h 30m
3h 12m
splan. meso
30 um z-max projection
1
2
3
I
neural tube cell
cell1
cell2
cell3
GFP intensity (AU)
t(mn)

Figure 6- figure supplement 1

A

Nkx2.5 eGFP

RERT$^{cre/-}$ *Rosa26Rtdtomato*$^{+/-}$

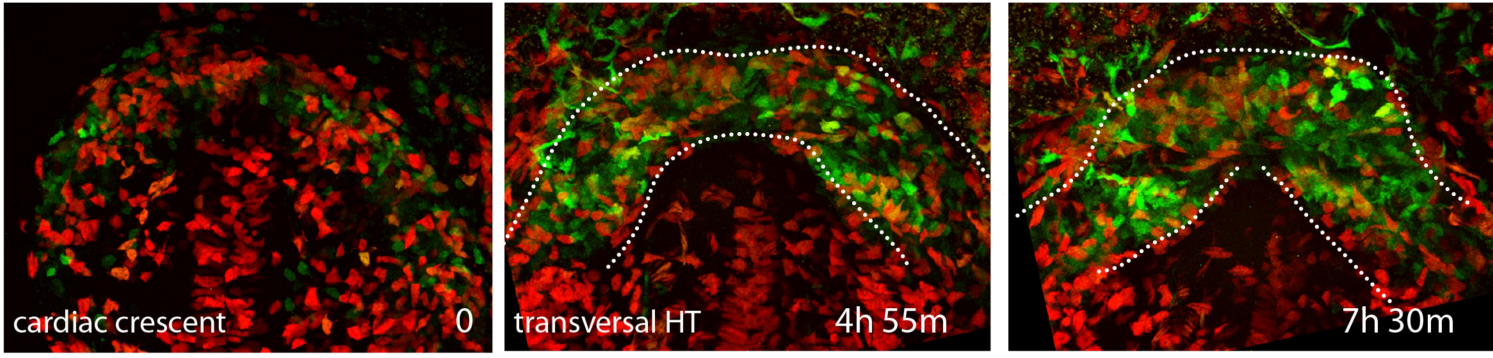

B

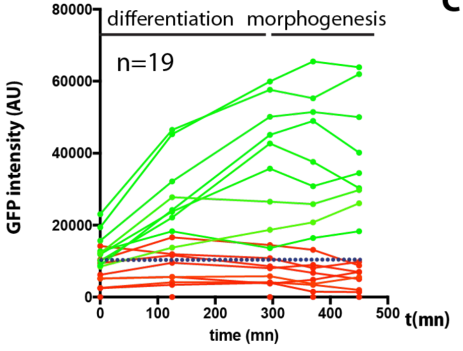

C

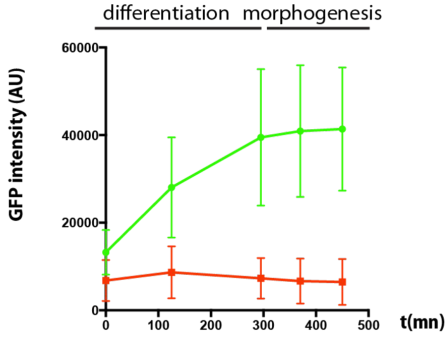

Figure 7

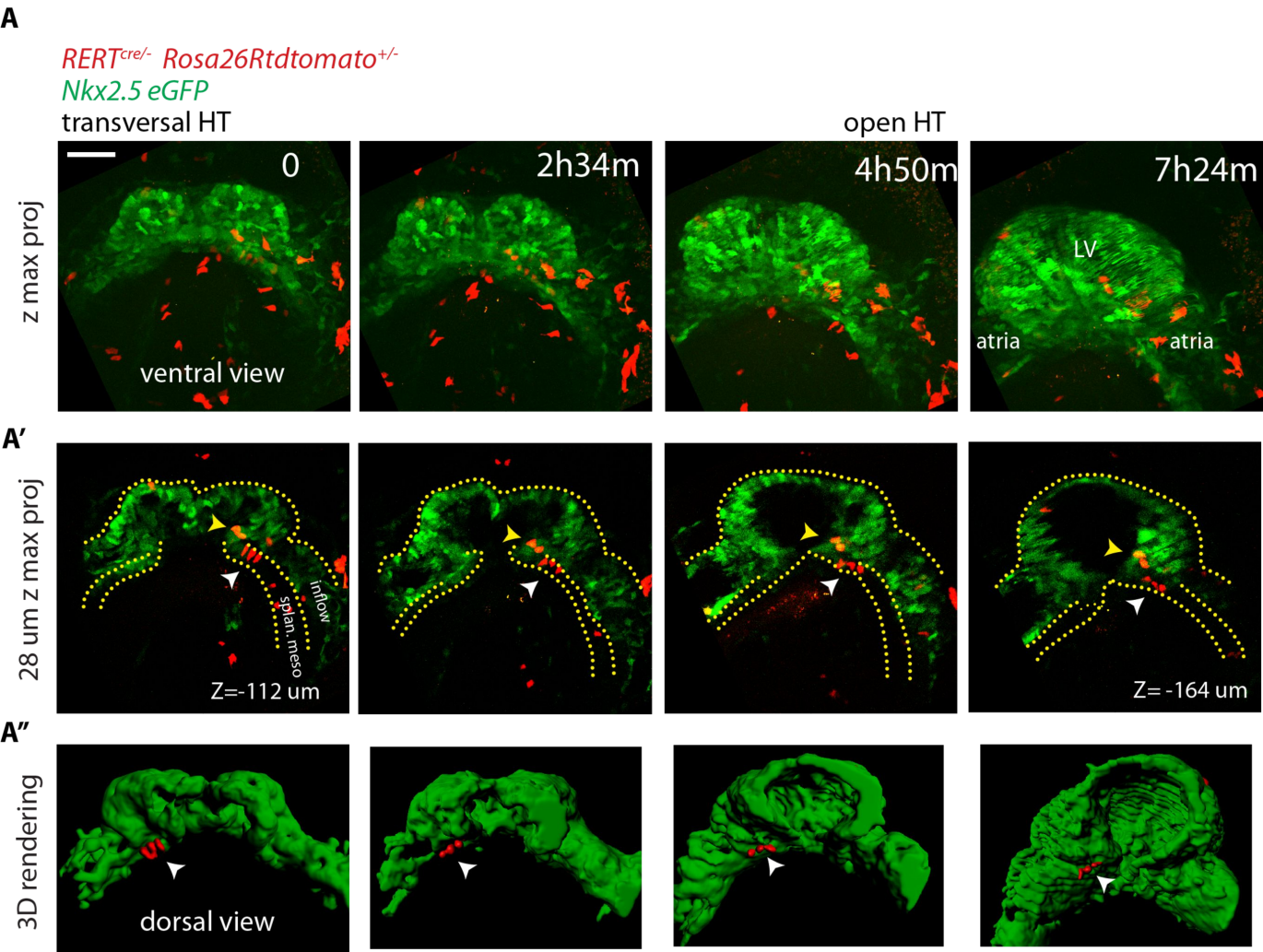
A
RERTcre/- Rosa26Rtdtomato+/-
Nkx2.5 eGFP
transversal HT
open HT
z max proj
0
2h34m
4h50m
7h24m
ventral view
LV
atria
atria
A'
28 um z max proj
inflow
splan. meso
Z=-112 um
Z= -164 um
A''
3D rendering
dorsal view

Figure 8

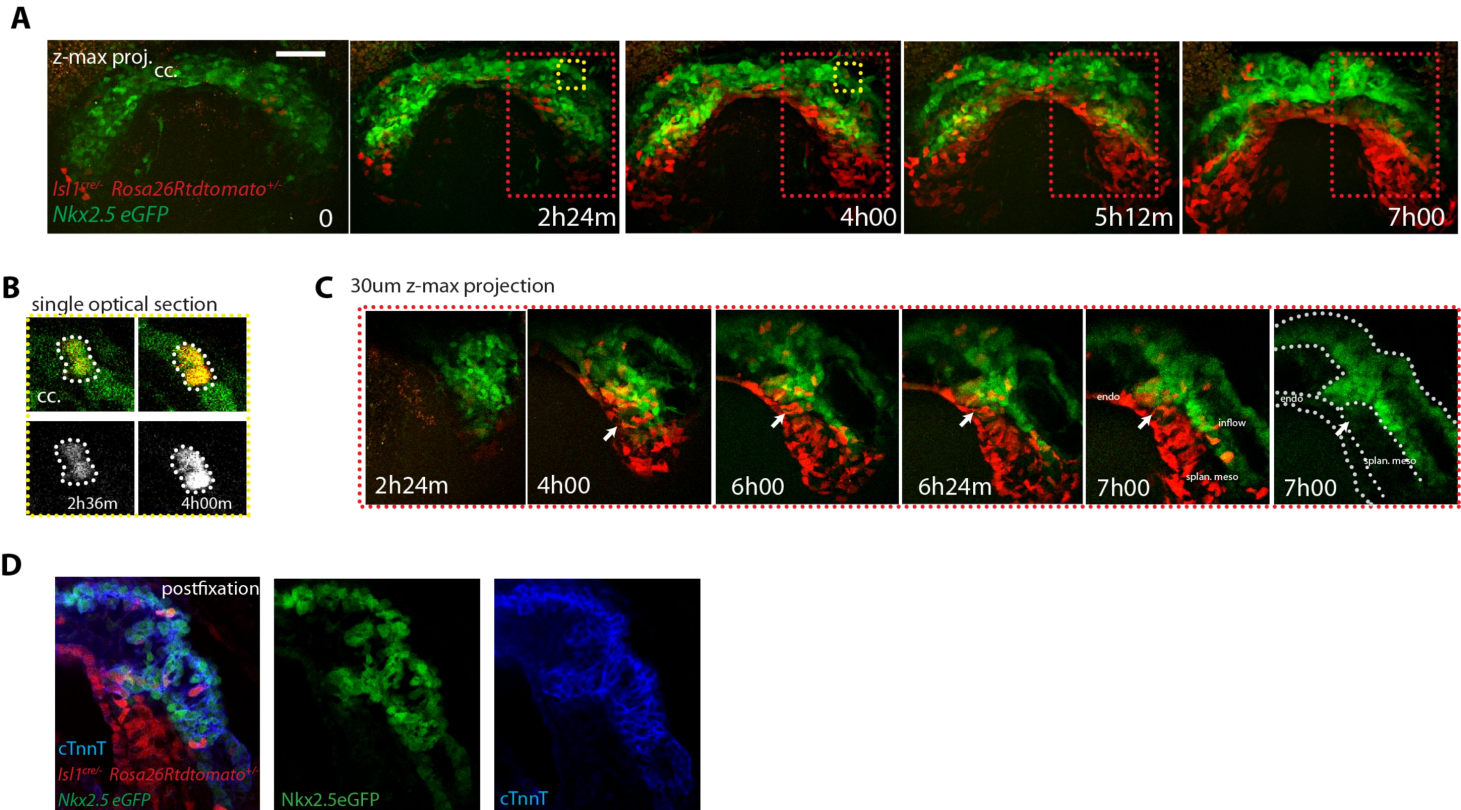
A
z-max proj.
cc.
Isl1cre/- Rosa26Rtdtomato+/-
Nkx2.5 eGFP
0
2h24m
4h00
5h12m
7h00
B
single optical section
cc.
2h36m
4h00m
C
30um z-max projection
2h24m
4h00
6h00
6h24m
7h00
endo
inflow
splan. meso
7h00
endo
splan. meso
D
postfixation
cTnnT
Isl1cre/- Rosa26Rtdtomato+/-
Nkx2.5 eGFP
Nkx2.5eGFP
cTnnT

Figure 8- figure supplement 1

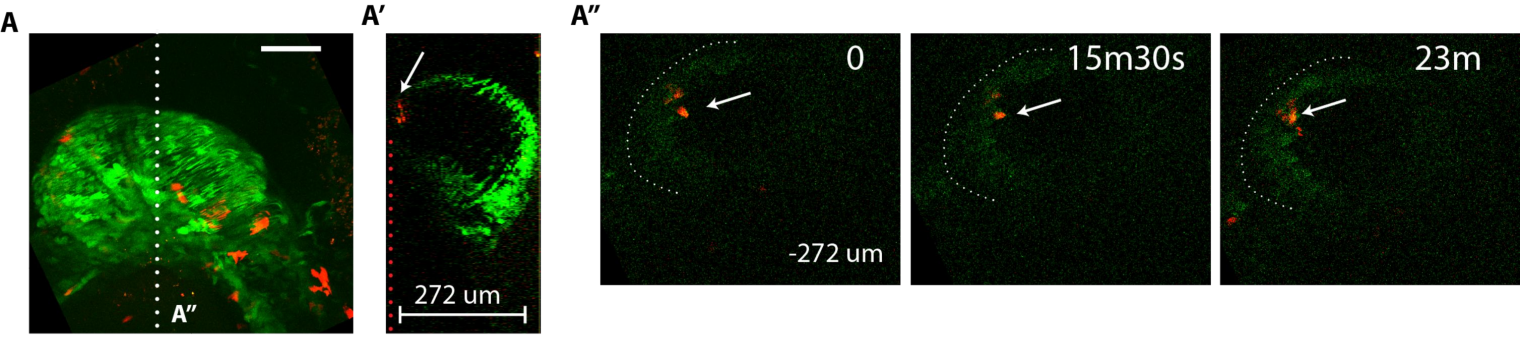

RERT$^{cre/-}$ Rosa26Rtdtomato$^{+/-}$
Nkx2.5 eGFP

Figure 8- figure supplement 2

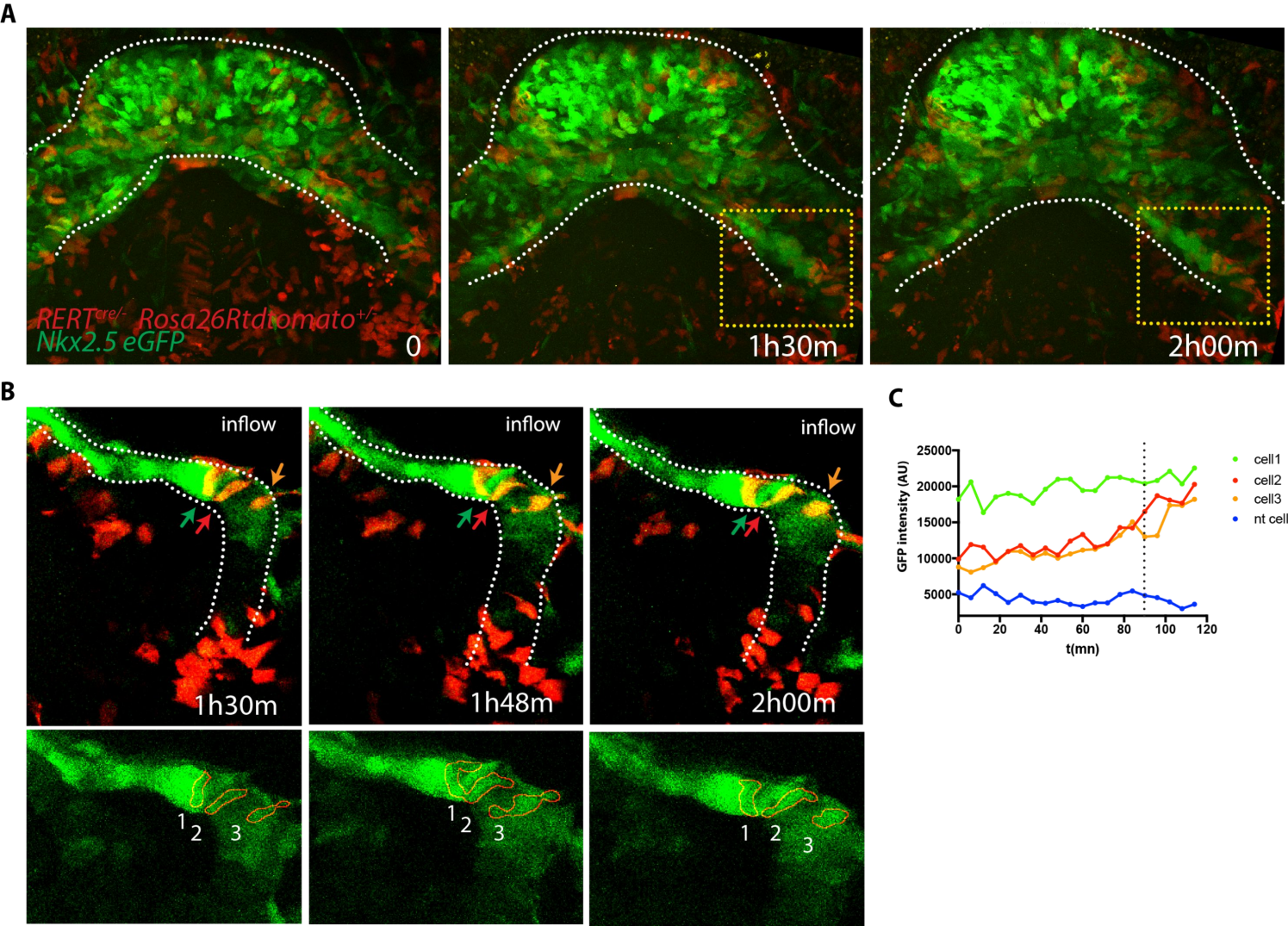

Figure 9

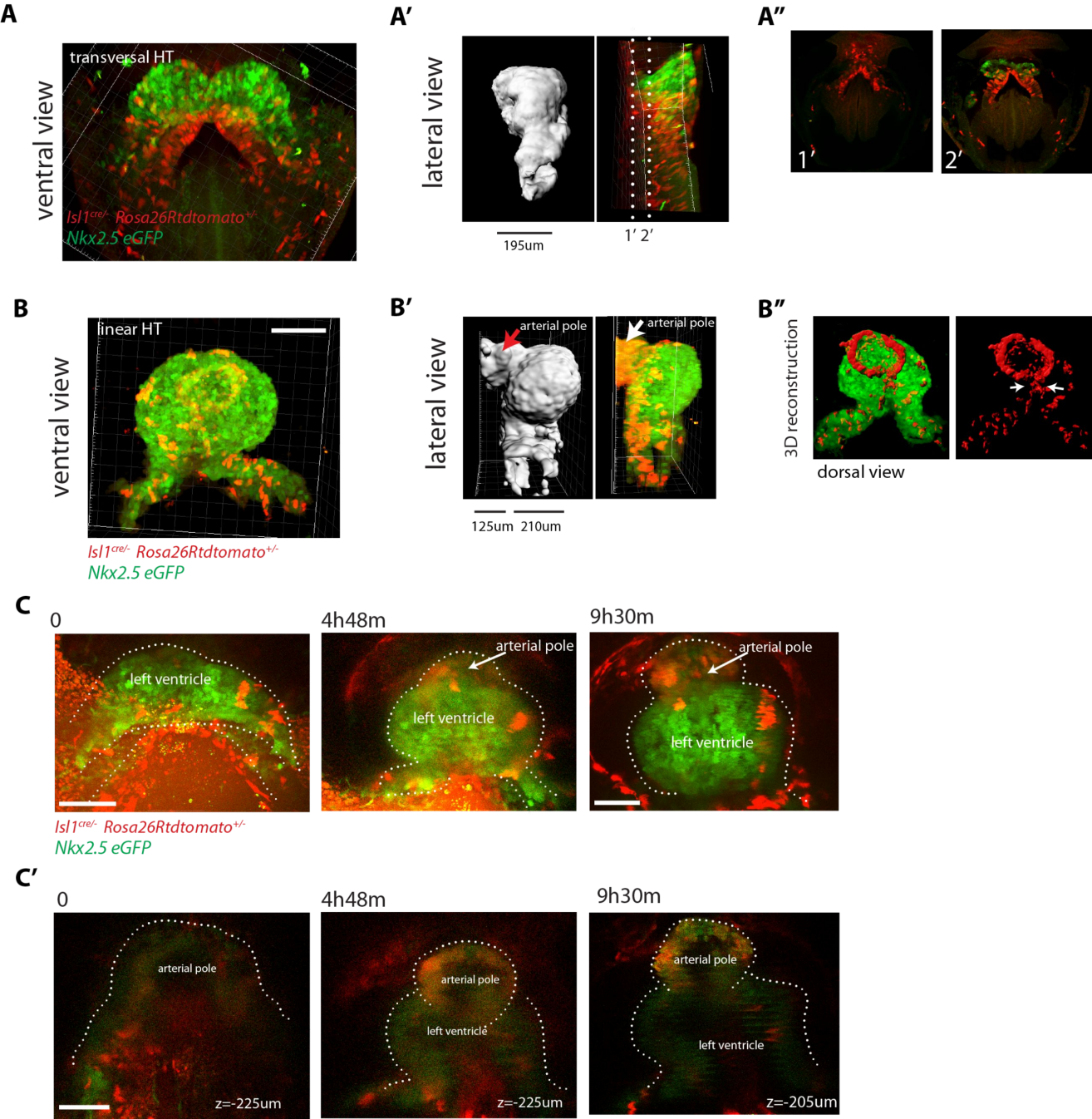
A
ventral view
transversal HT
Isl1cre/- Rosa26Rtdtomato+/-
Nkx2.5 eGFP
A′
lateral view
195um
1′ 2′
A″
1′
2′
B
ventral view
linear HT
Isl1cre/- Rosa26Rtdtomato+/-
Nkx2.5 eGFP
B′
lateral view
arterial pole
arterial pole
125um 210um
B″
3D reconstruction
dorsal view
C
0
4h48m
9h30m
left ventricle
arterial pole
left ventricle
arterial pole
left ventricle
Isl1cre/- Rosa26Rtdtomato+/-
Nkx2.5 eGFP
C′
0
4h48m
9h30m
arterial pole
z=-225um
arterial pole
left ventricle
z=-225um
arterial pole
left ventricle
z=-205um

Figure 10

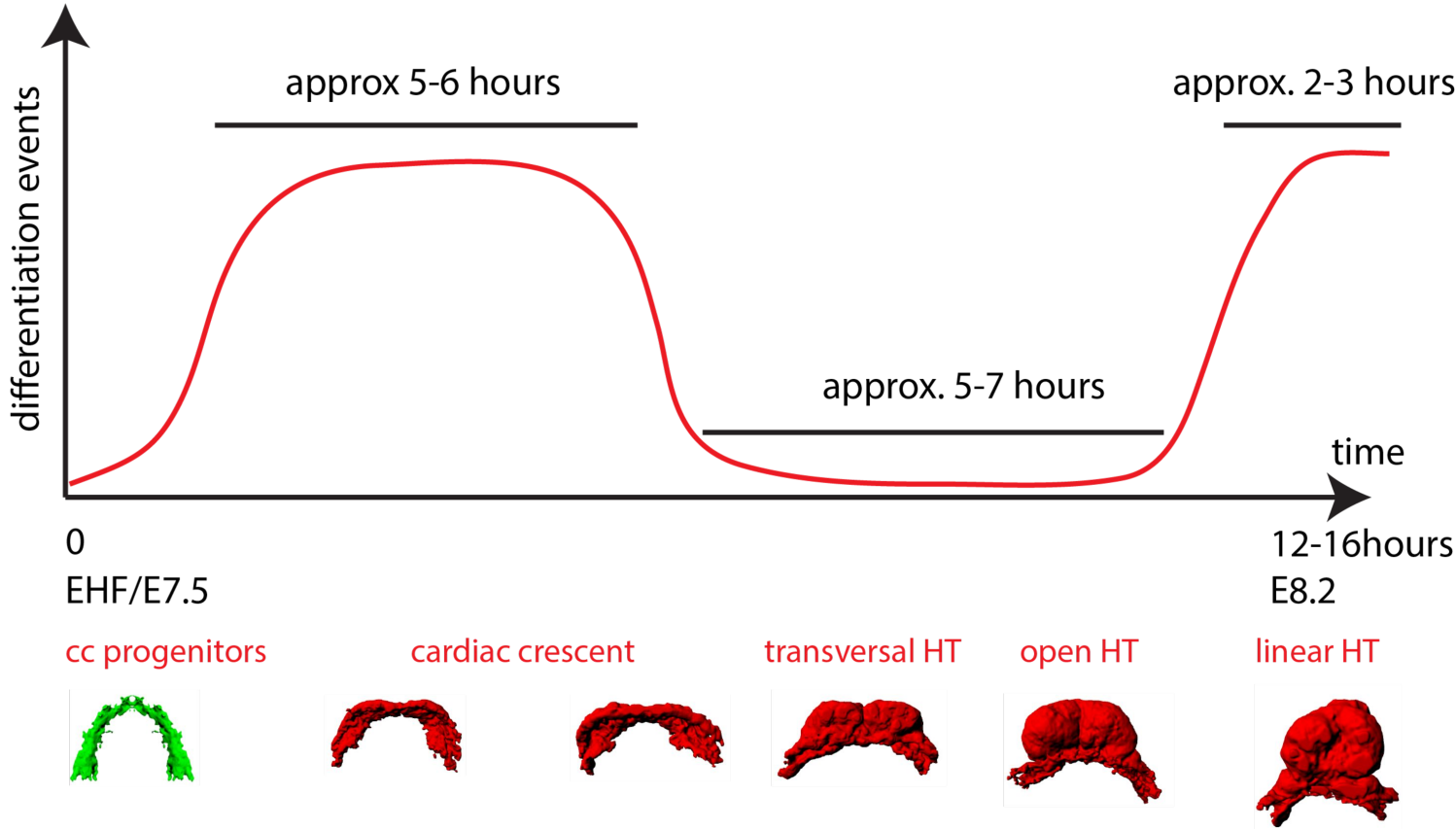
differentiation events
approx 5-6 hours
approx. 2-3 hours
approx. 5-7 hours
time
0
EHF/E7.5
12-16hours
E8.2
cc progenitors
cardiac crescent
transversal HT
open HT
linear HT